iScience

Article

A repeatedly evolved mutation in Cryptochrome-1 of subterranean animals alters behavioral and molecular circadian rhythms

Graphical abstract

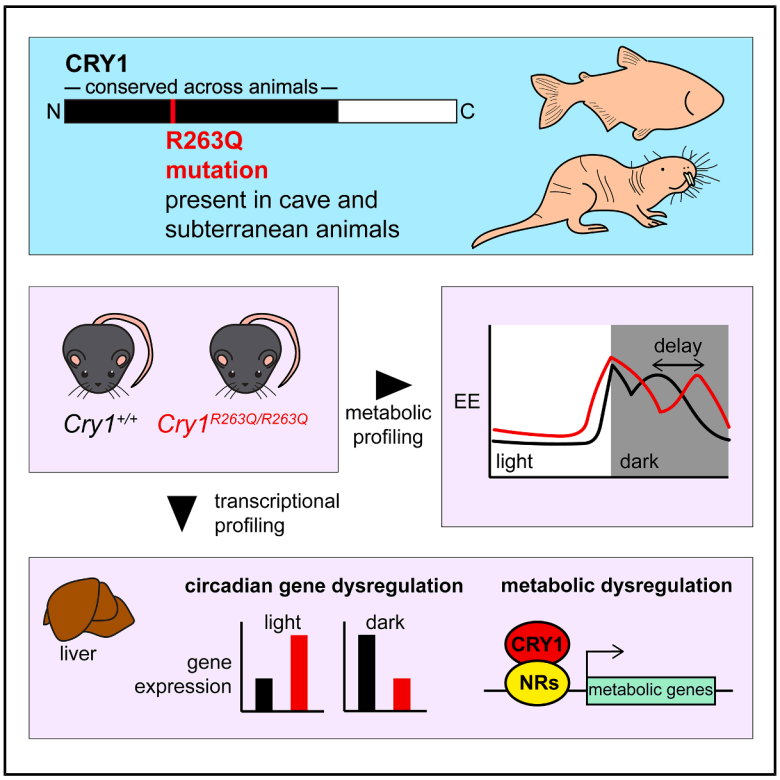

Authors

Amruta Swaminathan, Alexander Kenzior, Andrew Price, ..., NatiCia Morris, Alex C. Keene, Nicolas Rohner

Correspondence

nicolas.rohner@uni-muenster.de

In brief

Chronobiology; Evolutionary biology; Molecular biology; Zoology

Highlights

- The CRY1 R263Q mutation evolved repeatedly in subterranean lineages and may be adaptive
- *Cry1*$^{R263Q/R263Q}$ mice show delayed rhythms in energy expenditure and behavior
- *Cry1*$^{R263Q/R263Q}$ mice have dysregulated circadian oscillators in the liver
- The CRY1 R263Q mutation may impact transcriptional coregulation by CRY1 with nuclear receptors

Swaminathan et al., 2025, iScience *28*, 112874
July 18, 2025
https://doi.org/10.1016/j.isci.2025.112874

CellPress

iScience

CellPress
OPEN ACCESS

Article

A repeatedly evolved mutation in Cryptochrome-1 of subterranean animals alters behavioral and molecular circadian rhythms

Amruta Swaminathan,[1] Alexander Kenzior,[1] Andrew Price,[1] Hua Li,[1] Colin McCoin,[2] Aurélie Hintermann,[1] Kyle Weaver,[1] NatiCia Morris,[1] Alex C. Keene,[3] and Nicolas Rohner[1,2,4,5,*]

[1]Stowers Institute for Medical Research, Kansas City, MO 64110, USA
[2]Department of Cell Biology and Physiology, University of Kansas Medical Center, Kansas City, KS 66160, USA
[3]Department of Biology, Texas A&M University, College Station, TX 77840, USA
[4]Present address: Institute for Integrative Cell Biology and Physiology, University of Münster, Münster, 48149, Germany
[5]Lead contact
*Correspondence: nicolas.rohner@uni-muenster.de
https://doi.org/10.1016/j.isci.2025.112874

SUMMARY

Independent lineages showing similar phenotypic traits can use different genetic paths to achieve the same phenotypic outcome. Instances of such convergence at the genotypic level, however, remain underexplored. In this study, we generated and used a homozygous knock-in mouse model to characterize a previously identified mutation, CRY1 R263Q, that has repeatedly evolved in a highly conserved protein domain across lineages adapted to caves and subterranean environments. Indirect calorimetry experiments revealed that the mutation alters circadian patterns of energy expenditure, locomotor activity, and feeding behaviors in the dark phase, but no further metabolic phenotypes. We also found that the mutation causes the aberrant expression of canonical circadian and metabolic genes in the liver, consistent with circadian clock and metabolic dysregulation reported in subterranean dwellers, which may be adaptive in such environments. Our work highlights the capacity for selection to drive repeated phenotypic evolution through repetitions of the same underlying genetic change.

INTRODUCTION

Repeated evolution is the recurrence of similar phenotypic traits in multiple lineages. Often, these lineages inhabit similar environments and may face similar selection pressures to develop these traits.[1,2] The same developmental or physiological pathway can be perturbed at different points to produce the same gross phenotype and therefore genetic changes underlying repeated phenotypes are not necessarily the same in different lineages. However, instances of repeated evolution are also observed at the molecular level. Moran et al.[3] reported a mutation in the gene *Cryptochrome-1* (*Cry1*) that results in the substitution of an arginine (R) residue at position 263 in the CRY1 protein with a glutamine (Q) residue in a highly conserved domain (Figure 1A). Moreover, this mutation has arisen independently at least 5 times during animal evolution, in lineages that inhabit cave or subterranean environments (Figure 1B). Given that this specific mutation has repeatedly occurred in a highly conserved gene across species sharing similar environmental pressures, we hypothesize that it does not result simply in a loss of function but rather alters a specific function of the CRY1 protein. We refer to this mutation henceforth as the CRY1 R263Q mutation, or simply R263Q.

CRY1 is one of the major proteins regulating circadian rhythms,[5–9] which are intrinsically generated 24-h rhythms in the gene expression, physiology, metabolism, and behavior of an organism, and are ubiquitous across the tree of life.[10] Additionally, CRY1 also regulates glucose homeostasis, and lipid and steroid metabolic processes.[11–14] The animals that naturally carry the CRY1 R263Q mutation inhabit caves and underground burrows and are reported to have altered their circadian rhythms and metabolism.[15–26] One of the best-studied models of cave adaptation, the Mexican tetra *Astyanax mexicanus*, which carries the CRY1 R263Q mutation, has dysregulated its molecular circadian clock at least twice independently in two independent cave colonization events.[17,26] These cavefish also carry a nonsense mutation in *period2*, which codes for a close interacting partner of CRY1 and controls adipogenesis through its negative regulation of PPAR-gamma, leading to truncated transcripts.[27] Such dysregulation in transcriptional and behavioral rhythms has been suggested to aid in saving energy by eliminating rhythmic metabolism in nutrient-limited environments.[28] An unrelated species of cavefish, the Somalian cavefish *Phreatichthys andruzzii*, which also carries the CRY1 R263Q mutation, has completely lost its ability to entrain to light-dark cycles (but retains the ability to entrain to food cues[19,20]). Further, mutations have been reported in *P. andruzzii*'s *period2* ortholog as well.[18,27] In mammals, the naked mole-rat *Heterocephalus glaber* has phase-reversed expression of major circadian genes in comparison to

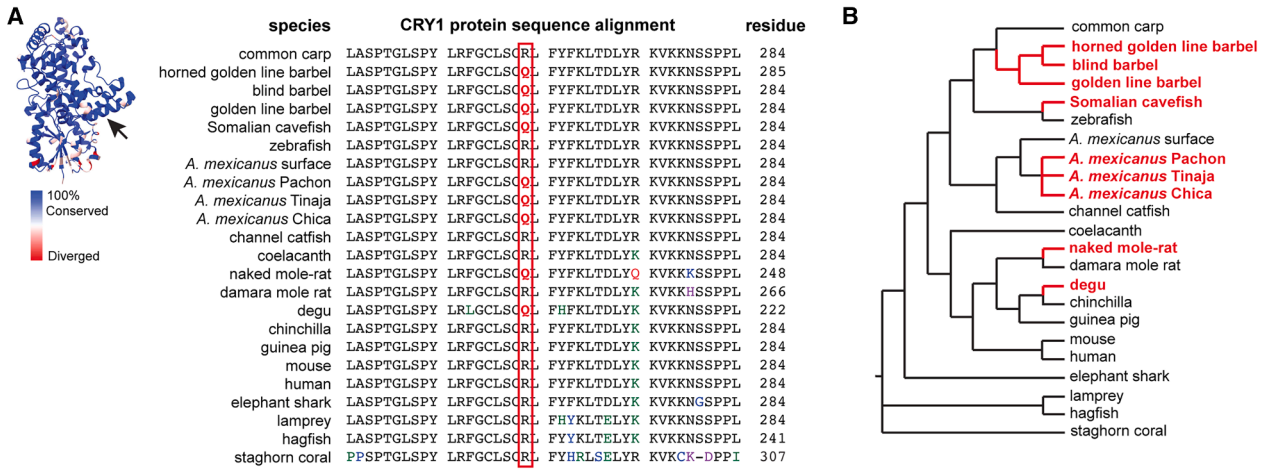

Figure 1. A mouse model to study the repeatedly evolved mutation in CRY1 orthologs of subterranean dwellers

(A) Partial amino acid sequence alignment of CRY1 orthologs from animal lineages including cnidarians, jawless fish, teleosts, and mammals. The red rectangle marks the site of the R263Q mutation, with the Q highlighted in boldface red font. Alignment redrawn from Moran et al.[3] licensed under CC BY-NC-ND 4.0. Colored residues indicate amino acid changes. Inset on the left is the crystal structure of mouse Cryptochrome-1 or CRY1 photolyase homology region (PDB: 7D0M). Colors indicate degree of amino acid conservation of mouse CRY1 with human CRY1, zebrafish CRY1a and *Xenopus* CRY1, with blue indicating 100% conservation and red indicating divergence. The arrow marks the position of the CRY1 R263Q mutation in the crystal structure. Structure visualized using ChimeraX 1.5rc202211120143.

(B) Animal phylogeny showing the occurrence of the CRY1 R263Q mutation. The branches in red are lineages in which the mutation has been detected. Phylogeny redrawn from Moran et al.[3] licensed under CC BY-NC-ND 4.0.

(C) Transcript and protein level expression of the mutant CRY1 R263Q locus. Left: plots of log2 values of mean counts per million (CPM) for total mRNA sequenced from CRY1 R263Q versus total mRNA sequenced from CRY1 WT male and female brain and liver tissues at ZT 12–13. The *Cry1* CPM value for each case is shown as a larger colored point on the plot (pink for the female plots and sky blue for the male plots). Right: Western blots showing CRY1 protein expression in the brain (top) and liver (bottom) tissues from wild-type and CRY1 R263Q mice, male and female. The positive control lanes are lysates prepared from U-2 OS CRY1/2 KO human cell lines transfected with an expression vector for mouse CRY1 (pSG5 backbone containing coding sequence for mouse CRY1 with FLAG, His and Myc epitope tags; pMC1SG5 vector as generated and described by Ye et al.[4]), and the negative control lanes are lysates prepared from untransfected U-2 OS CRY1/2 KO human cell lines. The CRY1 signal is shown in red (inside the yellow rectangles), and the GAPDH signal is shown in green as a loading control.

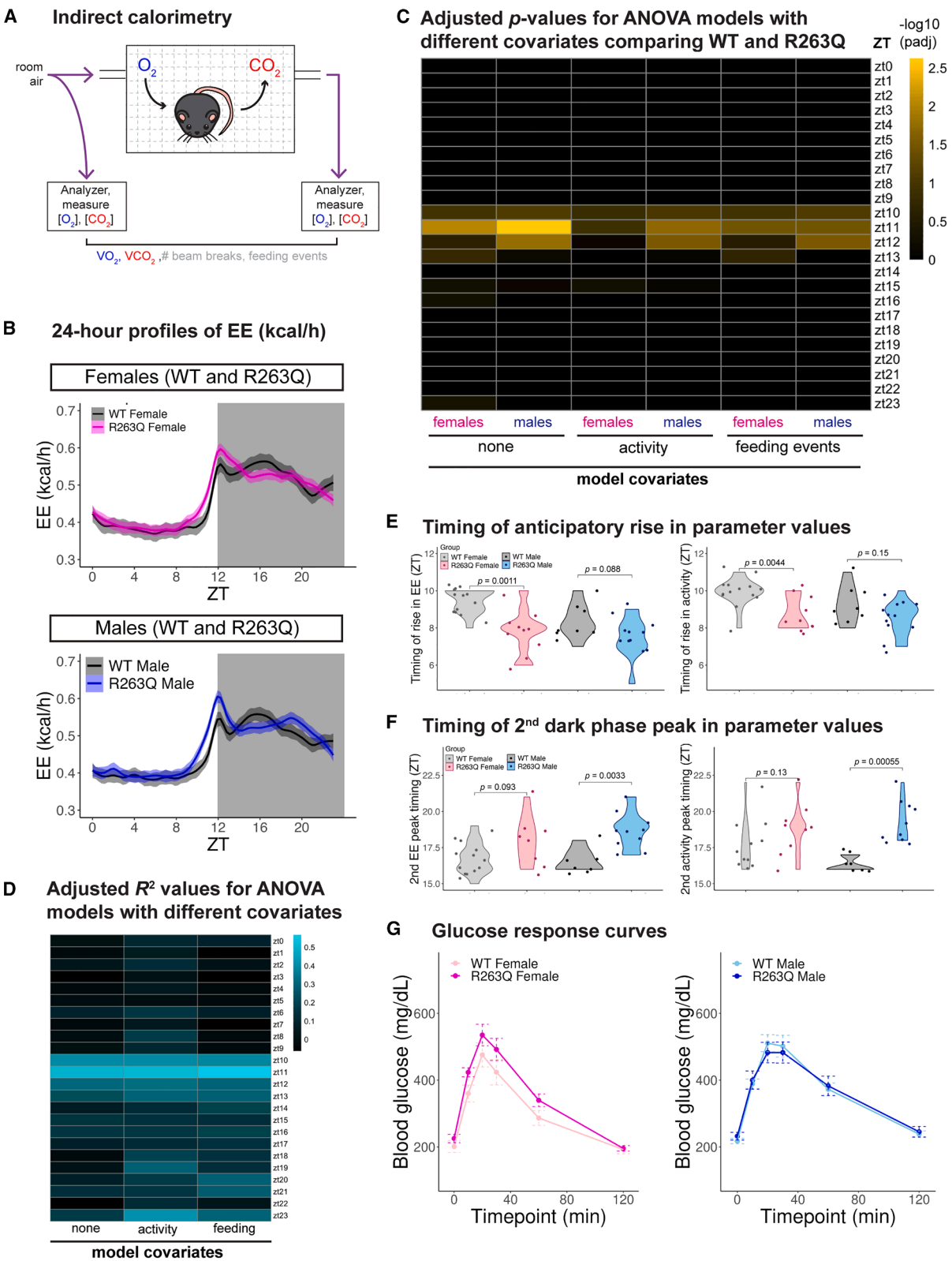

(legend on next page)

mice,[21] although they can show circadian activity patterns under a light-dark cycle.[22] Collectively, the repeated evolution of circadian clock dysregulation in independent lineages suggests that clock dysregulation leads to adaptive consequences for subterranean life.

The finding that the CRY1 R263Q mutation has evolved repeatedly in similar environments suggests a critical role for this mutation in such organisms. To explore this hypothesis, we have generated a mouse line carrying the CRY1 R263Q mutation. We found that CRY1 R263Q mice show delayed energy expenditure, locomotor activity, and feeding patterns in the dark phase, but not in the light phase. Gene expression analyses revealed the altered expression of major circadian and metabolic genes in the livers of the mutant mice. Taken together, our data suggest that the CRY1 R263Q mutation dysregulates the circadian clock at the transcriptional as well as behavioral levels and may thus aid in adaptation to subterranean life. In a broader context, our findings support the notion that the repeated evolution of phenotypes does not necessarily proceed by divergent genetic changes in independent lineages, and it is possible for shared environmental pressures to select for the same genetic change across independent lineages to drive the repeated evolution of a trait.

RESULTS

A mouse model for the repeatedly evolved CRY1 R263Q mutation

A mutation was recently reported in the gene *Cry1* to cause an amino acid substitution from a positively charged arginine to an uncharged polar glutamine in a protein domain that is otherwise highly conserved across metazoans[3] (Figure 1A). Moreover, this mutation has been detected in several species of cave-dwelling fish, namely, *A. mexicanus*, *Sinocyclocheilus* spp., *P. andruzzii*, and in two burrowing mammals, the naked mole-rat *H. glaber*, and the degu *Octodon degus*. Therefore, the CRY1 R263Q mutation has arisen independently at least 5 times during animal evolution (Figure 1B). Given that this specific mutation has repeatedly occurred in a highly conserved gene, in species that share similar environmental pressures, we hypothesize that this mutation does not result simply in a loss of function. Rather, it might target a specific function of this protein.

To test this hypothesis and investigate the function of the CRY1 R263Q mutation, we used CRISPR-Cas9 to introduce the underlying G788A nucleotide substitution at the endogenous *Cry1* locus of the mouse genome (Figures S1A and S1B, also see STAR Methods). We performed RNA sequencing (RNA-seq) using brain and liver tissues collected at zeitgeber time (ZT) 12–13 from wild-type (WT) and R263Q adult mice from both sexes and confirmed that *Cry1* mRNA expression is not abrogated in these organs in R263Q individuals (Figure 1C, left). We then performed western blotting with brain and liver lysates from WT and R263Q mice from both sexes using CRY1 antibodies to confirm comparable CRY1 protein expression between WT and R263Q individuals (Figure 1C, right; Figure S1C, $p = 1$ for comparing WT and R263Q female brain as well as liver samples, $p = 0.8$ for comparing WT and R263Q male brain samples and $p = 0.2$ for comparing WT and R263Q male liver samples, Wilcoxon test, $n = 3$ for each group). Consequently, we conclude that the CRY1 R263Q mutation does not impact the normal transcription and translation of the *Cry1* gene i.e., it does not phenocopy a CRY1 loss-of-function at the level of gene or protein expression.

CRY1 R263Q mice manifest delayed energy expenditure and locomotor activity patterns in the dark phase relative to wild-type mice

Since CRY1 is a key regulator of mammalian circadian rhythms and metabolism, we screened the CRY1 R263Q mice and WT controls for altered behavioral and metabolic parameters using indirect calorimetry (IC, see STAR Methods and Figure 2A; $n = 14$ WT females, 10 R263Q females, 8 WT males and 12 R263Q males). We collected O_2 and CO_2 measurements (mL/min) to infer energy expenditure (EE), as well as locomotor activity (or simply activity) patterns measured as infrared beam breaks in the x- and y-directions, and feeding events (see STAR Methods for details). We observed no significant changes to gross EE, locomotor activity or feeding frequency (number of feeding events) in the R263Q mice over a full day or during specific photoperiods (Figure S2), except for a slight increase in daytime feeding in R263Q males in comparison to WT (Figure S2C, $p = 0.016$, Wilcoxon test, $n = 8$ WT males and 12 R263Q males).

We then hypothesized that the CRY1 R263Q mutation may cause changes to the circadian *patterns* of variation in metabolism and behavior, rather than to the gross measurements of such parameters over a 12- or 24-h photoperiod. To refine the temporal resolution of our analyses, therefore, we examined EE, activity, and feeding events hourly over the course of a 24-h day. We computed the mean values for hourly EE, activity, and feeding events across all the experiment days for each

Figure 2. CRY1 R263Q individuals show changes to 24-h EE profiles, but no defects in glucose metabolism

(A) Graphic of metabolic phenotyping using indirect calorimetry (IC).

(B) 24-h profiles of EE as a function of ZT. Solid lines represent means of hourly values computed for all individuals in an experimental group and shaded areas indicate 95% confidence intervals around the means. Top: females; bottom: males. Gray rectangles from ZT12-ZT24 represent the dark phase.

(C) Adjusted *p*-values for ANOVA models with different covariates comparing ZT-wise EE values for WT and R263Q individuals, separated by sex. Colors indicate -log10(adjusted *p*-value) as shown in the color scale.

(D) Adjusted R^2 values for ANOVA models in (C). Colors indicate -log10(adjusted *p*-value) as shown in the color scale.

(E) Violin plots comparing the timings (measured in ZT) of the anticipatory rise in EE (left) and activity (right) at the end of the light phase.

(F) Violin plots comparing the timings (measured in ZT) of the second peak in EE (left) and activity (right) during the dark phase.

For 2E-F, the width of the violin plots represents the density of data points at the corresponding *y* values, and the overlaid scatter represents individual data points. *p*-values are computed using the Wilcoxon test.

(G) Glucose response curves showing blood glucose levels (in mg/dL) as a function of time elapsed since glucose injection. Left: females; right: males. Points represent mean glucose levels for each group at a given time point, and the error bars represent standard error.

mouse and visualized the values as a function of zeitgeber time (ZT) (Figures 2B and S3A).

We asked if the mutants showed any detectable changes to the circadian rhythmicity of hourly EE. We focused on EE since it is the final response variable used as a metabolic readout. For this analysis, we used Kronos, an R-based tool for assessing circadian rhythmicity in biological datasets.[29] Using Kronos, we modeled the hourly EE as a decomposition of sine and cosine components, and as a function of ZT with the period parameter set to 24 h. The Kronos analysis yielded sinusoid curves fitted to each dataset (WT females, R263Q females, WT males, and R263Q males), with much of the variance in the data explained by the fitted curves, and very similar acrophase values (Table S1). Based on this, we concluded that all 4 groups examined in this study show clear circadian rhythmicity in their hourly EE patterns. However, we noticed that the sinusoid curves fitted by Kronos were overly smooth and failed to capture important features of the data that are seen in the mean EE plots (Figure 2B), such as the initial sharp peak in EE around ZT12 for all the groups, and the second shallower peak (Figure S3B). Therefore, we did not proceed further with Kronos to compare the rhythmicities of the WT and R263Q EE patterns. Instead, we opted to fit an analysis of variance (ANOVA) model to compare the EE patterns between WT and R263Q animals of the same sex.

First, we sought to verify if the criteria for ANOVA are fulfilled by our dataset. Although the EE, activity, and feeding events for each individual were measured independently of each other, it is reasonable to expect that activity and feeding event patterns, both energy-consuming tasks, would directly impact the EE patterns over the course of a 24-h day. Indeed, we saw that both activity and feeding events were highly correlated with EE patterns (Figure S4A, Pearson correlation coefficients indicated on the respective correlation plots). Therefore, we decided to treat activity and feeding events as covariates while attempting to fit an ANOVA model to the dataset with genotype (WT and R263Q) and sex as independent variables. We found that the genotype had a significant effect on the EE at ZT10-12, while sex did not have an effect at any timepoint (Figure S4B; Tables S2 and S3). Activity and feeding events both significantly influenced the EE at a few ZT values, with activity having an impact on more ZT values than the feeding events. Since ZT11 showed the strongest effect of the genotype, we plotted the residual Q-Q plot at ZT11 (Figure S4C) and saw that the data points fall along a straight line. This indicates that the assumptions for performing an ANOVA analysis are valid.

Based on the above, we proceeded to fit ANOVA models to compare EE values between WT and R263Q individuals at all ZTs. We fit three ANOVA models, one with no additional covariates and two to include activity and feeding events as covariates to assess if the differences found in EE, if any, were attributable to the variation in these covariates. The ANOVA model with no covariate showed significant differences in EE at ZT11 between WT and R263Q females, and at both ZT11 and 12 between WT and R263Q males (Figure 2C and Table S4). Activity, when included as a covariate, could explain the difference in EE for females, but not for males. Feeding events, on the other hand, could not fully explain the difference in EE for either sex. Indeed, this was reflected in the R^2 values for each of the three models, with the highest R^2 values across ZTs obtained when activity was used as a covariate (Figure 2D and Table S5). From this analysis, we conclude that the 24-h EE profiles when compared ZT-wise are not significantly different between genotypes except at the onset of the dark phase, and this difference can be explained at least in part by underlying differences in the 24-h activity patterns.

We noted that for all groups, the EE remains relatively constant up to ~ ZT9, and then rapidly rises to form a peak between ZT9-12, just before the onset of the dark phase (Figure 2B). We measured the timing of this anticipatory rise in EE for each individual and saw that R263Q females achieved this rise significantly sooner than WT females (Figure 2E, left; $p = 0.0011$, Wilcoxon test, $n = 13$ WT females and 10 R263Q females). No such difference, however, was detectable for the males ($p = 0.088$, Wilcoxon test, $n = 8$ WT males and 11 R263Q males). These patterns were also reflected in the activity profiles (Figure 2E, right; for females, $p = 0.0044$, Wilcoxon test, $n = 14$ WT and 10 R263Q; for males, $p = 0.15$, Wilcoxon test, $n = 8$ WT and 12 R263Q). We further noted that after the first peak in EE close to the dark phase onset, there is a second, shallower peak in the dark phase (Figure 2B). We found that the timing of this second peak in EE was significantly delayed in R263Q males compared to wild-type males, with no such differences evident in females (Figure 2F, left; for males, $p = 0.0033$, Wilcoxon test, $n = 7$ WT and 10 R263Q; for females, $p = 0.093$, Wilcoxon test, $n = 13$ WT and 8 R263Q). These trends were also reflected in the activity profiles (Figure 2F, right; for males, $p = 0.00055$, Wilcoxon test, $n = 7$ WT and 10 R263Q; for females, $p = 0.13$, Wilcoxon test, $n = 11$ WT and 9 R263Q).

Next, we also compared respiratory exchange ratios (RER) between male and female genotypes. We did not detect any differences either in the photoperiod average analysis (Figure S5A) or in the 24-h profiles (Figure S5B). Overall, IC analyses show that R263Q mutants show higher EE values than WT at ZT11 for females, and ZT11 and 12 for males, with this difference partially explained by activity patterns at the same ZTs, and a significant delay in the second peak of EE and activity in the case of R263Q males compared to WT males.

Mutating or depleting mouse CRY1 has been previously reported to cause hyperglycemia and inability to regulate blood glucose levels following a glucose challenge.[12,14,30] This phenotype is present in Mexican cavefish that naturally harbor the R263Q mutation, raising the possibility that this mutation disrupts glucose tolerance.[15] To test this hypothesis, we compared R263Q and WT mice using a standard glucose tolerance test (see STAR Methods and Figure S5C). We found no significant differences in fasting blood glucose levels between WT and R263Q individuals of either sex (Figure S5D; $p = 0.35$ for comparing WT and R263Q females, $p = 0.34$ for comparing WT and R263Q males, Wilcoxon test, $n = 9$ WT females, 7 R263Q females, 9 WT males and 7 R263Q males). After a glucose challenge, all groups showed the expected increase in blood glucose levels in the first 30 min and were able to tolerate glucose and regulate blood glucose back to fasting levels within 2 h of the glucose challenge (Figure 2G; $n = 9$ WT females, 7 R263Q females, 9 WT males and 7 R263Q males). These data,

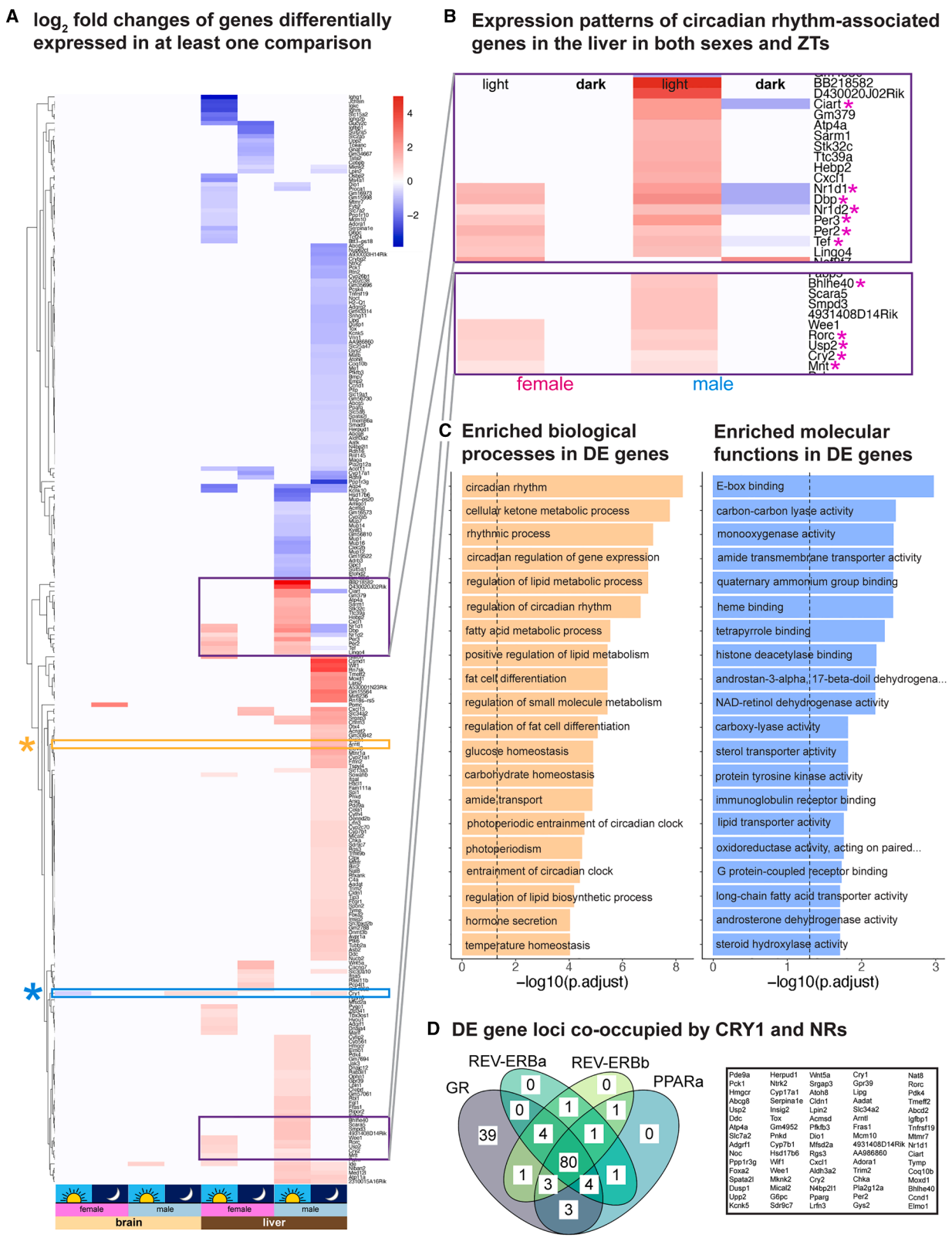

(legend on next page)

therefore, do not provide any evidence of insulin resistance or impaired glucose homeostasis capacity in the R263Q mice.

In summary, male mice carrying the CRY1 R263Q mutation exhibited an increase in EE at ZT11 and 12, as well as a delay in their energy expenditure patterns during the dark phase. R263Q females show an increase in EE at ZT11, an advance in the anticipatory rise in EE before the dark phase, but no significant delays in EE patterns in the dark phase. Locomotor activity patterns could reasonably explain the EE patterns. Finally, the R263Q mice do not have deficits in glucose metabolism as assayed by a standard glucose tolerance test.

CRY1 R263Q mice show dysregulation of circadian and metabolic genes in the liver

We next sought to examine the effects of the CRY1 R263Q mutation on gene expression to determine if it could explain the altered behavioral patterns observed by IC. Since we were assaying for both circadian and metabolic phenotypes, we selected the brain and liver to perform RNA-seq and compare WT and R263Q mice to call differentially expressed (DE) genes. Moreover, since circadian and metabolic gene expression profiles can vary depending on the time of day and can be set by external cues, we sampled brain and liver tissue at two different ZTs – onset of the dark phase (ZT 12–13) and onset of the light phase (ZT 22–23). Finally, sex can also influence circadian rhythms and metabolism.[31,32] To ensure that the DE genes detected are indeed a consequence of the genotype, we controlled for tissue type, sex and sampling time by comparing WT and R263Q samples from the same sex and tissue type and collected at the same time to call DE genes. This resulted in 8 comparisons (2 sexes, 2 tissue types and 2 sampling times) across the datasets to identify DE genes between genotypes (Figure S6A). A summary heatmap showing the fold changes of all the DE genes in the R263Q samples relative to WT under all the different conditions is shown in Figure 3A.

We found that the brain tissues showed almost no genotype-specific expression, regardless of sex or time of sampling/ZT (Figure 3A, the left four columns). One gene was differentially expressed per comparison in the brain tissues. Interestingly, *Cry1* itself was downregulated in R263Q female brains at the onset of the light phase but showed no differential expression at the onset of the dark phase. By contrast, for males, while *Cry1* was not differentially expressed in the brain at the onset of the light phase, it was upregulated in R263Q samples at the onset of the dark phase (Figure 3A, blue rectangle with blue asterisk).

The liver tissues showed a much more pronounced transcriptional response to the R263Q mutation than the brain. In general, the number of DE genes called was higher in the male samples than the female samples across all conditions. Of note, we found very few genes that were differentially regulated in the same direction (up or down) at both sampling times, indicating that the R263Q mutation's transcriptomic effects depend on the ZT. Also, most of the genes identified as differentially regulated at one sampling time are not identified as such at the other sampling time. This is consistent with the fact that CRY1 is a circadian rhythm regulator whose levels vary throughout the course of a 24-h day, resulting in circadian variation in the expression of the genes that it regulates.

Very interestingly, we found one cluster in the male liver samples that contains DE genes showing the strongest response to sampling time. These genes were *up*regulated in R263Q samples at the onset of the light phase but were *down*regulated at the onset of the dark phase. These genes turned out to be canonical regulators of circadian rhythms,[8] mostly *repressors* which also regulate metabolism (Figure 3B). In this group we found nuclear receptor subfamily 1 group D members 1 and 2, *Nr1d1* and *Nr1d2*, which function in a feedback loop auxiliary to the core circadian feedback loop consisting of the clock circadian regulator (*Clock*), basic-helix-loop-helix ARNT-like 1 (*Bmal1* or *Arntl*), *Cry* and period circadian clock (*Per*) genes and fine-tune this core loop.[8,33] *Nr1d1* and *Nr1d2* are transcribed by *Bmal1*, and the resulting proteins, the REV-ERBs, inhibit the transcription of *Bmal1*. We also found the D site albumin promoter binding protein (*Dbp*) and thyrotroph embryonic factor (*Tef*) genes, which are transcribed by the core circadian transcription factors CLOCK and BMAL1, and code for proline and acidic amino acid-rich basic leucine zipper (PAR-bZIP) transcription factors that participate in a second auxiliary circadian feedback loop, besides regulating the expression of several metabolic genes.[8] We also found the circadian associated receptor of transcription (*Ciart*) gene, predicted to be a regulator of circadian gene expression.[34] In the same cluster, we also found that *Per2* and *Per3* were upregulated at the onset of the light phase but not differentially expressed at the onset of the dark phase. The *Per* genes code for PER proteins that function alongside the CRY proteins as repressors of the circadian clock.[4,8,35] We found a few other major circadian repressors in a different cluster following a pattern similar to the *Per* genes – basic-helix-loop-helix family member e40 (*Bhlhe40*), cryptochrome-2 (*Cry2*) and max-binding protein (*Mnt*) which function by inhibiting *Bmal1*

Figure 3. RNA-seq analysis shows dysregulation of circadian and metabolic genes in the liver

(A) Heatmap of log2 fold change values for all genes identified as DE in at least one comparison of R263Q vs. WT. Fold changes are calculated from the contrasts shown in Figure S6A. The order of the comparisons from left to right is: female brain at the onset of the light phase; female brain at the onset of the dark phase; male brain at the onset of the light phase; male brain at the onset of the dark phase; female liver at the onset of the light phase; female liver at the onset of the dark phase; male liver at the onset of the light phase; male liver at the onset of the dark phase. Colors indicate -log10(adjusted *p*-value) as shown in the color scale.

(B) Expression patterns of DE circadian rhythm-associated genes in the liver. Expanded from (A).

(C) GO pathway enrichment analysis for all DE genes shown in (A). The vertical dotted lines represent the threshold of adjusted p-value < 0.05 (Fisher's exact test).

(D) Venn diagram showing DE gene loci co-occupied by CRY1 and various NRs. The list of genes co-occupied by CRY1 and all four NRs examined is provided on the right.

For samples collected at the onset of the light phase, n = 6 WT female brain samples, 5 R263Q female brain samples, 5 WT male brain samples, 6 R263Q male brain samples, 5 WT female liver samples, 6 R263Q female liver samples, 5 WT male liver samples, and 5 R263Q male liver samples.

For samples collected at the onset of the dark phase, n = 4 WT female brain samples, 4 R263Q female brain samples, 6 WT male brain samples, 5 R263Q male brain samples, 5 WT female liver samples, 5 R263Q female liver samples, 7 WT male liver samples, and 6 R263Q male liver samples.

transcription or BMAL1-mediated transactivation.[8,36–38] This cluster also contained RAR-related orphan receptor gamma (*Rorc*) which codes for one of the ROR proteins that form a positive transcription-translation feedback loop with *Bmal1*[8]; and ubiquitin-specific peptidase 2 (*Usp2*), which has roles in photic entrainment, locomotor circadian rhythms, and nuclear accumulation of the PER1 protein.[39–42] We also saw that several of the genes described above – *Nr1d1*, *Nr1d2*, *Dbp*, *Tef*, *Per2*, *Per3*, *Cry2*, *Mnt* and *Usp2* – show similar patterns in female liver samples. Notably, when we examined *Cry1* levels in the liver, we observed an opposite pattern of expression in male liver samples, but consistent patterns in female liver samples (Figure 3A, blue rectangle and blue asterisk). When we searched for the differential expression of canonical circadian activators in the liver, we found that *Arntl* (or *Bmal1*) showed a pattern opposite to that of most of the repressors described above, but similar to *Cry1* – it was not differentially regulated in male livers at the onset of the light phase but was *up*regulated at the onset of the dark phase (Figure 3A, gold rectangle and gold asterisk). *Clock*, the other circadian activator, was not found to be differentially expressed under any conditions.

We performed a Gene Ontology (GO) pathway enrichment analysis on the entire set of DE genes, the results of which are shown in Figure 3C. Seven out of the top 20 biological processes enriched in the list of DE genes (including the most significantly enriched biological process) were related to circadian rhythms. This agrees with the large number of differentially regulated circadian genes that we found and described in Figures 3A and 3B. Other enriched biological processes were mostly related to metabolism, such as cellular ketone metabolism, lipid metabolism, glucose and carbohydrate metabolism, hormone metabolism, and small molecule metabolism. These enriched biological pathways point to a general disruption of circadian rhythms and metabolic pathways in the livers of R263Q mice. The top enriched molecular functions in the list of DE genes were consistent with the enriched biological processes. The most significantly enriched molecular function was E-box binding, which is the promoter element bound by core circadian transcription factors,[43,44] followed by a slew of various types of metabolic enzyme activity terms. These include monooxygenase activity, (characteristic of the cytochrome P450 enzymes,[45] many of which are differentially regulated in the liver samples), heme binding, sterol and lipid transporter activity, ligand-activated transcription factor activity, and FAD binding.

Nuclear receptors (NRs) regulate metabolic pathways by transcribing genes in response to ligands.[11,46] Since CRY1 is known to influence transcription independently of CLOCK:BMAL1 by functioning as a corepressor with nuclear receptors,[11,46] we asked if the disrupted metabolic pathways enriched in our dataset could be explained by the interaction of CRY1 with nuclear receptors. We overlapped publicly available lists of genomic loci co-occupied by CRY1 and various nuclear receptors in the liver[46] with our list of DE genes in the liver. Intriguingly, we found that over 50% (134 out of 249) of our DE genes were co-occupied by CRY1 and the glucocorticoid receptor (GR), 37% (93 out of 249) were co-occupied by CRY1 and PPARa, and 36.5% (91 out of 249) each were co-occupied by CRY1 and REV-ERBa, and CRY1 and REV-ERBb. 32% (80 out of 249) of the DE genes in the liver were found to be shared occupancy sites for CRY1 and all the above-mentioned NRs and are involved in diverse metabolic pathways including glucose metabolism, lipid metabolism and xenobiotic detoxification (Figure 3D). This suggests that the CRY1 R263Q mutation might impact CRY1's normal co-repressor activity with several NRs at a shared set of genomic loci.

We also repeated the GO pathway enrichment analysis for subsets of DE genes in the liver based on sex and sampling time to identify classes of genes that are differentially regulated by genotype in a sex- and ZT-dependent manner (Figure S6B). We found that at the onset of the light phase, circadian rhythm terms were among the most significantly enriched biological processes regardless of sex, along with the enrichment of relevant molecular functions such as ''transcriptional coregulator binding'', ''transcriptional corepressor binding'', and ''nuclear receptor activity'' in both sexes; ''photoreceptor activity'', ''nuclear receptor binding'', and ''FAD binding'' in females, and ''E-box binding'' in males. This agrees with our visual inspection of the DE gene list (Figures 3A and 3B) and the GO pathway analysis for the entire DE gene list (Figure 3C). Additionally, in females, a few genes coding for immunoglobulin proteins were downregulated, as evidenced by enriched molecular functions ''immunoglobulin receptor binding'', ''immunoglobulin binding'', and ''antigen binding''. In the male samples, several genes involved in lipid metabolism such as fatty acid binding protein 5 (*Fabp5*), sphingomyelin phosphodiesterase 3 (*Smpd3*), and pyruvate dehydrogenase kinase isoenzyme 4 (*Pdk4*)[47–49]; hormone secretion such as G protein-coupled receptor 39 (*Gpr39*) and cholinergic receptor muscarinic receptor 3 (*Chrm3*)[50,51]; and glucose homeostasis were upregulated. Genes downregulated in males included the major urinary protein (*Mup*) gene family, the deletion of which shifts mouse metabolism to an anabolic state,[52] the cytochrome P450 enzyme *Cyp2a5* which regulates heme metabolism, and hydroxysteroid 17-beta dehydrogenase 6 (*Hsd17b6*) which is involved in androgen catabolism[53,54] (Table S6).

At the onset of the dark phase, enriched biological processes in females included those related to solute transport, such as solute carrier family 34 member 2 (*Slc34a2*); and genes regulating steroid metabolism, such as retinol dehydrogenase 9 (*Rdh9*) and cytochrome P450 gene *Cyp17a1*.[55,56] Other important metabolic genes were also seen to be dysregulated, such as lipin 2 (*Lpin2*) that regulates lipid metabolism genes.[57] In males, a variety of metabolic processes were enriched. The upregulated genes included the arginine vasopressin receptor 1a (*Avpr1a*), which contributes to rhythmic behavior in mice,[58] Dopa decarboxylase (*Ddc*) that may be involved in the synthesis of the sleep-regulating hormone melatonin,[59] melatonin receptor 1a (*Mtnr1a*) that is associated with instances of type II diabetes,[60,61] forkhead box A2 *(Foxa2*) that is involved in glucose homeostasis and fat metabolism,[62,63] insulin-induced gene 2 (*Insig2*) that regulates cholesterol biosynthesis,[64] genes regulating hormone metabolism such as arylsulfatase G (*Arsg*),[65] and a few cytochrome P450 genes *Cyp21a1*, *Cyp7b1* and *Cyp2c70* that are involved in various metabolic and detoxification processes and interact with the circadian clock.[66] The downregulated genes included nocturnin (*Noct*), which in humans is under

circadian control and regulates metabolism by dephosphorylating NADPH[67]; lipid metabolism regulators such as peroxisome proliferator activated receptor gamma (*Pparg*), a master regulator of adipocyte differentiation,[68] lipase G, endothelial type (*Lipg*), aldehyde dehydrogenase 3 family member A2 (*Aldh3a2*), and ATP-binding cassette subfamily D member 2 (*Abcd2*)[69–71]; glucose and glycogen homeostasis regulators such as phosphoenol pyruvate carboxykinase 1 (*Pck1*), fructose 2,6-bisphosphatase 3 (*Pfkfb3*), glycogen synthase 2 (*Gys2*), protein phosphatase 1 regulatory subunit 3G (*Ppp1r3g*),[72–75]; and regulators of cholesterol and sterol metabolism including phospholipid transfer protein (*Pltp*) and ATP binding cassette subfamily G member 5 (*Abcg5*).[76,77] Other downregulated genes included coenzyme Q10b (*Coq10b*) which is involved in cellular respiration[78] and *Hsd17b6* (Table S7).

To summarize, RNA-seq analyses showed almost no transcriptomic changes in the brain. The liver, on the other hand, showed a strong transcriptomic response to the R263Q mutation. Several metabolic regulatory genes are differentially expressed, often in a context-specific manner depending on the sex and the sampling time, which is not surprising given that metabolic regulation is known to be sexually dimorphic[31,32] and many metabolic genes are under circadian control,[79] which is sensitive to ZT. Nevertheless, two major trends emerge from this analysis: (1) the R263Q mutation exerts profound, sex-independent effects on the liver circadian oscillator itself, and (2) the R263Q mutation results in the misexpression of several metabolic genes that are under the transcriptional control of NRs.

DISCUSSION

In this study, we investigated the transcriptomic, behavioral, metabolic, and physiological consequences of a repeatedly evolved mutation (R263Q) in the circadian protein Cryptochrome-1, or CRY1. This mutation resides in a highly conserved domain of the protein and is seen to recur specifically in animal lineages that have adapted to low-light environments such as caves and subterranean burrows. We developed a mouse model that is homozygous for the CRY1 R263Q mutation and carried out an in-depth metabolic phenotyping to uncover the potential effects of this mutation. We found a change in 24-h EE profiles in CRY1 R263Q mutants that are at least partially explained by underlying changes in activity patterns, but no change to glucose metabolism capacity. Finally, RNA sequencing revealed disruption in expression patterns of several canonical circadian and metabolic genes in the liver. Through this study, we have demonstrated the power of a single nucleotide substitution to orchestrate change not only at the level of gene expression, but also at the level of the whole organism.

The CRY1 R263Q mutation dysregulates the liver circadian clock

RNA-seq showed virtually no transcriptomic differences in the brains of WT and R263Q mice. The brain contains the central circadian pacemaker, and other subregions of the brain also have their own circadian clocks, which can run with phases shifted relative to the master clock.[80] This could explain why we detected no transcriptomic differences in the brain in our datasets, since we used entire brain hemispheres for RNA extraction.

However, we found significant differences between liver samples collected from WT and R263Q mice. The most enriched class of genes was circadian rhythm genes, and indeed, we saw several genes that participate in the molecular circadian oscillator showing disrupted expression. Our data are therefore consistent with a dysregulated liver circadian oscillator. The R263Q mutation resides close to the FAD-binding domain of CRY1.[3] FAD-binding is known to stabilize CRY1,[81] while the ubiquitin ligase complex SCF^{FBXL3} competes for the same binding pocket and marks CRY1 for proteasomal degradation, thereby destabilizing it.[82] The CRY1 R263Q mutation may be altering this balance between FAD and SCF^{FBXL3} and impacting the stability of the CRY1 protein, which could, in turn, dysregulate the dynamics of the molecular oscillator.

The pattern of dysregulation is also interesting – except for *Cry1* itself, most of the circadian repressor genes (*Cry2*, *Per2*, *Per3*, *Nr1d1*, and *Nr1d2*) were upregulated at the onset of the light phase and downregulated at the onset of dark phase (in the case of males, and not DE for females). By contrast, the circadian activator *Arntl* (or *Bmal1*) was not DE at the onset of the light phase but was upregulated at the onset of the dark phase. All these transcripts are known to show 24-h oscillations in the mouse liver. Interestingly, the circadian repressor genes noted above have been reported to exhibit mRNA peaks a few hours before or at the onset of the dark phase, and troughs near the light phase in the WT mouse liver.[83,84] In our dataset, these genes are unchanged/downregulated in the R263Q liver at the onset of the dark phase, close to the time the mRNAs are reported to peak in the WT liver, and they are upregulated in the R263Q liver at the onset of the light phase, close to the time the mRNAs are reported to trough in the WT liver. This is also true of *Dbp* and *Tef,*[85] which function in an auxiliary circadian feedback loop. Similarly, *Arntl* mRNA is reported to trough at the onset of the light phase,[83] and our dataset shows that it is upregulated at this time of day. These observations are consistent with a circadian oscillator in the liver that is either damped or phase-shifted (Figure S7). 24-h metabolic phenotyping showed a delay in energy expenditure, activity, and feeding patterns in the dark phase in R263Q male mice. Therefore, it is possible that the R263Q mutation impacts the stability of CRY1, resulting in a phase-shifted oscillator that causes delayed patterns of behavior. This hypothesis can be validated by comparing the affinities of the CRY1 WT and R263Q proteins for FAD, as well as by sampling the liver transcriptomes at multiple circadian time points.

It is interesting to note additionally that the CRY1 R263Q mutation appears to impact males more than it does females. Sex-dependent differences in circadian rhythms, metabolism, and physiology, which are largely driven by underlying anatomical and hormonal differences, have been reported in the literature.[31,86] One study reported that CRY1 and its paralog CRY2 are necessary to sustain sexual dimorphism in the mouse liver by regulating growth hormone (GH) cycling.[87] This study found that several cytochrome P450 genes (*Cyp2b9*, *Cyp2d9*, *Cyp4a12,* and *Cyp7b1*) that show sexually dimorphic expression in the liver show feminized expression profiles in *Cry*-deficient

male mice. Moreover, *Cry*-deficient males showed other defects associated with sexually dimorphic GH patterns, such as reduced body weight and downregulation of major urinary protein (*Mup*) genes. Our data do not show the differential regulation of the *Cyp* genes considered in this study. In fact, *Elovl3,* which is highly expressed in the male liver and is reduced in *Cry*-deficient mice as reported in,[87] is upregulated in the R263Q male liver. Further, we compared body weights between WT and R263Q mice aged ~2 months (Figure S8, $n = 9$ WT females, 7 R263Q females, 9 WT males, and 8 R263Q males), well beyond the age of 2–3 weeks at which growth deficits began to become apparent in *Cry*-deficient mice.[87] We found no difference among genotypes in the female mice ($p = 0.09$, Wilcoxon test), and in fact, the R263Q males show a slight increase in body weight in comparison to wild-type males ($p = 0.046$, Wilcoxon test). These inconsistencies with the report on *Cry*-deficient mice could be due to the CRY1 R263Q mutation not phenocopying a full loss-of-function (see further in the discussion), and also because the *Cry2* locus is intact in our mouse model. However, we did find several members of the *Mup* gene cluster downregulated in the R263Q male liver (Figure 3A), consistent with the report for *Cry*-deficient mice. Additionally, our data also show that *Cyp17a1* and *Hsd17b6,* which are involved in androgen biosynthesis and catabolism, respectively,[54,56] are downregulated in the R263Q male liver. *Cyp17a1*-deficient mice are phenotypically female despite an XY genotype.[88] Overall, our data suggest that the CRY1 R263Q mutation has sex-specific effects, which could be caused in part by the differential modulation of *Mup* gene expression, and by the downregulation of specific androgen metabolism-associated genes. These sex differences are likely attributable to physiological and metabolic differences between the sexes that create different contexts for the function of WT CRY1 and the R263Q mutated version. Future experiments deleting the *Cry1* locus in both male and female animals will serve to tease out the precise differential roles CRY1 plays in each sex and the mechanisms by which these roles are orchestrated in the different physiological backgrounds.

The CRY1 R263Q mutation could be a partial loss-of-function or a neofunctionalization

The evolutionary convergence of the CRY1 R263Q mutation suggests that it does not represent a complete loss of function and might instead be selected for. *Cry1*$^{-/-}$ mice show a shortened free-running period relative to WT mice,[5–7] which is also reflected in the molecular rhythms of the *Per1* gene.[7] CRY1 R293H substitution leads to a shortened molecular rhythm, suggesting a hypomorphic phenotype.[89] There are also other mutations in the literature that suggest a CRY1 hypermorphic phenotype. CRY1 C414A substitution or an in-frame deletion of 24 amino acids coded in exon 11 both lead to a period-lengthening phenotype.[90,91]

The CRY1 R263Q mutation, which we have characterized in this study, does not clearly phenocopy either the full loss of function, the hypomorph or the hypermorph phenotype. First, we performed a glucose tolerance test on our CRY1 R263Q mice and detected no signs of hyperglycemia or glucose intolerance, consistent with our conclusion that the CRY1 R263Q mutation does not mimic a canonical loss of function.[92] Second, even the full *Cry1*$^{-/-}$ deletion does not show any discernible alterations to circadian wheel-running patterns in a light/dark cycle, ostensibly due to the masking effect of light.[5] The CRY1 R263Q mutation, however, shows an activity pattern phenotype even under a light/dark cycle. It seems, therefore, that the effect of this mutation is strong enough not to be masked by light. Therefore, we believe we are at risk of only underestimating, rather than overestimating, the phenotypic effects of the CRY1 R263Q mutation. To the best of our knowledge, this is unlike any CRY1 mutation described thus far and supports our hypothesis that the CRY1 R263Q mutation may be a neofunctionalization. Future studies on mice kept in constant darkness will help tease out the effects of the mutation on the intrinsic oscillator.

How does the CRY1 R263Q mutation contribute to subterranean adaptation?

It is possible that circadian clock dysregulation in low-light environments could be a consequence of relaxed selection, as has been argued for several cave-associated traits (reviewed in[93]). If it was indeed a case of relaxed selection, however, then it is extremely unlikely that the very same mutation would occur independently in multiple lineages. This supports the possibility that the R263Q mutation in CRY1 was selected for due to some adaptive advantage. Cave-dwelling species such as the Mexican cavefish *A. mexicanus* and the Somalian cavefish *P. andruzzii* are reported to have dysregulated circadian clocks,[17,19,26,94,95] which could be a combination of drift and selection. A dysregulated circadian clock has been suggested to be adaptive for the cave ecotype of *A. mexicanus* in many ways – by conserving energy in a nutrient-limited environment by eliminating rhythmic metabolism,[28] or by contributing to reduced sleep duration[17] or increased wakefulness which could be a beneficial foraging strategy to find and consume more food in such food-scarce environments. Additionally, *A. mexicanus* also shows a suite of metabolic traits that resemble disease phenotypes in the human context, such as insulin resistance and increased fat accumulation.[15,16,27,96] Therefore, an advantage could also be conferred by an indirect effect of CRY1 on dysregulating metabolism and creating metabolic disease-like phenotypes. Our transcriptomic analysis leads to the hypothesis that the CRY1 R263Q mutation disrupts the normal interaction of CRY1 with NRs, leading to broad transcriptional changes in metabolic genes across the liver transcriptome. Future work will examine the precise mechanisms by which the CRY1 R263Q mutation dysregulates molecular and behavioral rhythms and assess its adaptive value in a low-light environment.

Taken together, we have generated a knock-in mouse harboring a CRY1 mutation that has evolved independently multiple times in fish and mammals. The availability of this mouse line enables a systematic investigation of the functional differences, which may ultimately help shed light on the adaptive nature of these changes. Our study represents the first functional characterization of a novel, repeatedly evolved mutation in lineages that inhabit cave and subterranean environments. Our analyses provide evidence for changes in metabolic and circadian regulation at multiple levels of organization, providing the basis for future studies examining the role of CRY1 in the repeated evolution of adaptation to low-light environments. Moreover,

while the phenomenon of repeated evolution of similar phenotypic traits in response to similar environmental pressures or constraints is not an unfamiliar one, the underlying genetic bases for these shared phenotypes remain elusive. Often, different genetic pathways involved in producing the same phenotype are modified in different lineages to give rise to a nevertheless convergent phenotype. Our work, however, highlights the possibility that the very same genetic change can underlie parallel phenotypic changes. In a broader context, our work supports the notion that shared selective pressures can act by favoring the same genotype repeatedly in multiple lineages to drive the evolution of a shared phenotypic trait.

Limitations of the study

One of the limitations of this study is the lack of indirect calorimetry data collected under conditions of total darkness. Recording in total darkness is used to dissect different components of the observed circadian clock dysregulation phenotype, such as changes to the period of the intrinsic oscillator or changes to the light response pathway. This would permit narrowing the cause(s) of the phenotype. However, according to the pain and distress classification categories (B-E) of the Institutional Animal Care and Use Committees of the Stowers Institute and the University of Kansas Medical Center (IACUCs), recording animals in darkness constitutes a category E procedure i.e., activities that cause pain and distress for which pain- and distress-relieving measures are not implemented. For this reason, approvals for total darkness experiments were not granted. However, we observed a subtle phenotype despite recording animals in a light-dark cycle – a phenomenon that is not observed even in the full *Cry1* loss-of-function mutant due to the masking effects of light, as discussed. For this reason, we believe that we are at worst underestimating, and not overestimating, the effects of the mutation. Another limitation is the use of a nocturnal species, i.e., mice, as a model to study the CRY1 R263Q mutation. We opted to use a mouse model due to the poor efficiency of homologous recombination-based gene editing in fish, as well as the availability of sophisticated metabolic phenotyping equipment for rodents. However, this leaves open the question of what the implications of this mutation are for a diurnal species such as the surface ecotype of *A. mexicanus*. Nocturnal and diurnal species use similar mechanisms to generate circadian rhythms in the brain, and the differences have been linked to the mechanism of firing of neurons in the suprachiasmatic nucleus (SCN) of the brain.[97] Given that the CRY1 R263Q mutation impacts the circadian gene circuitry, therefore, we would hypothesize that the effects of the mutation would be largely conserved between nocturnal and diurnal species. However, further experiments are required to verify this hypothesis. A third limitation of the study is that we have focused on just one of the many mutations known to affect circadian genes in subterranean dwellers. We have therefore not been able to capture the suite of circadian and metabolic dysregulation phenotypes displayed by subterranean animals. However, our study has allowed us to isolate the effects of the CRY1 R263Q mutation alone. Further studies will focus on mutations in other circadian genes to functionally dissect the mechanisms of circadian clock disruption in cave and subterranean animals.

RESOURCE AVAILABILITY

Lead contact

Requests for further information and resources should be directed to and will be fulfilled by the lead contact, Nicolas Rohner (nicolas.rohner@uni-muenster.de).

Materials availability

Mouse lines generated in this study are available from the lead contact with a completed materials transfer agreement.

Data and code availability

- Original data underlying this article have been deposited in the Stowers Original Data Repository at the following link: https://www.stowers.org/research/publications/libpb-2490. The raw fastq files for the RNA-seq datasets are available in the Gene Expression Omnibus (GEO) database under the accession number GSE277611. The gene count tables generated from the RNA-seq datasets are available as supplemental tables.
- Original codes underlying this article have been deposited in the Stowers Original Data Repository at the following link: https://www.stowers.org/research/publications/libpb-2490.
- Any additional information required to reanalyze the data is available from the lead contact upon request.

ACKNOWLEDGMENTS

We would like to thank members of the Rohner lab, particularly Fanning Xia, and faculty members of the Graduate School of the Stowers Institute for Medical Research, Dr. Ariel Bazzini, Dr. Matthew Gibson, Dr. Ron Yu, and Dr. SaraH Zanders for regular inputs and feedback on the project. We acknowledge the following members of various technology centers at the Stowers Institute for Medical Research for their valuable services – Heidi Monnin, Marina Thexton and Lana Worthen for animal maintenance and experimental assistance; Madelaine Gogol for general inputs on RNA-seq and statistical analyses; Andrea Moran, Brandon Miller and MaryEllen Kirkman for helping create the CRY1 R263Q line; Sean McGrath and Michael Peterson for generating RNA-seq libraries and sequencing reads; Olga Kenzior, Fengyan Deng and Chongbei Zhao for generating controls to validate the anti-CRY1 antibodies used in this study; and the Media Prep and Glassware facilities. We also thank Dr. Achim Kramer (Charité – Universitätsmedizin Berlin, Germany) for kindly sharing the U-2 OS BLH CRY1/2 KO cell line, and Dr. Aziz Sancar and Dr. Christopher Selby (University of North Carolina Chapel Hill, NC, USA) for kindly sharing the pMC1/2SG5 plasmids coding for CRY1/2 that were used to generate antibody controls. We are also grateful to the Metabolic and Obesity Phenotyping (MORPh) facility at the University of Kansas Medical Center, particularly Dr. John Thyfault, for discussing the data interpretation with us. This work was supported by the Stowers Institute for Medical Research, and National Institutes of Health grants 1DP2AG071466–01, R24OD030214, P20GM144269 and SIFAR S10 grant S10OD028598. This work was performed as part of thesis research for A.S. at the Graduate School of the Stowers Institute for Medical Research.

AUTHOR CONTRIBUTIONS

A.S., A.K., A.H., A.C.K., and N.R. designed research; A.S., C.M., K.W., and N. M. performed research; A.S., A.P., and H.L. analyzed data; and A.S., A.H., and N.R. wrote the article.

DECLARATION OF INTERESTS

The authors declare no competing interests.

STAR★METHODS

Detailed methods are provided in the online version of this paper and include the following:

- KEY RESOURCES TABLE
- EXPERIMENTAL MODEL AND STUDY PARTICIPANT DETAILS

SUPPLEMENTAL INFORMATION

Supplemental information can be found online at https://doi.org/10.1016/j.isci.2025.112874.

Received: December 18, 2024
Revised: April 30, 2025
Accepted: June 8, 2025
Published: June 12, 2025

REFERENCES

1. Losos, J.B. (2011). Convergence, adaptation, and constraint. Evolution *65*, 1827–1840.
2. Bolnick, D.I., Barrett, R.D., Oke, K.B., Rennison, D.J., and Stuart, Y.E. (2018). (Non)Parallel Evolution. Annu. Rev. Ecol. Evol. Syst. *49*, 303–330.
3. Moran, R.L., Jaggard, J.B., Roback, E.Y., Kenzior, A., Rohner, N., Kowalko, J.E., Ornelas-García, C.P., McGaugh, S.E., and Keene, A.C. (2022). Hybridization underlies localized trait evolution in cavefish. iScience *25*, 103778.
4. Ye, R., Selby, C.P., Ozturk, N., Annayev, Y., and Sancar, A. (2011). Biochemical analysis of the canonical model for the mammalian circadian clock. J. Biol. Chem. *286*, 25891–25902.
5. van der Horst, G.T., Muijtjens, M., Kobayashi, K., Takano, R., Kanno, S., Takao, M., de Wit, J., Verkerk, A., Eker, A.P., van Leenen, D., Buijs, R., et al. (1999). Mammalian Cry1 and Cry2 are essential for maintenance of circadian rhythms. Nature *398*, 627–630.
6. Kume, K., Zylka, M.J., Sriram, S., Shearman, L.P., Weaver, D.R., Jin, X., Maywood, E.S., Hastings, M.H., and Reppert, S.M. (1999). mCRY1 and mCRY2 are essential components of the negative limb of the circadian clock feedback loop. Cell *98*, 193–205.
7. Griffin, E.A., Jr., Staknis, D., and Weitz, C.J. (1999). Light-independent role of CRY1 and CRY2 in the mammalian circadian clock. Science *286*, 768–771.
8. Takahashi, J.S. (2017). Transcriptional architecture of the mammalian circadian clock. Nat. Rev. Genet. *18*, 164–179.
9. Laothamatas, I., Rasmussen, E.S., Green, C.B., and Takahashi, J.S. (2023). Metabolic and chemical architecture of the mammalian circadian clock. Cell Chem. Biol. *30*, 1033–1052.
10. Dunlap, J.C. (1999). Molecular bases for circadian clocks. Cell *96*, 271–290.
11. Koike, N., Yoo, S.H., Huang, H.C., Kumar, V., Lee, C., Kim, T.K., and Takahashi, J.S. (2012). Transcriptional architecture and chromatin landscape of the core circadian clock in mammals. Science *338*, 349–354.
12. Jang, H., Lee, G., and Kim, J.B. (2017). SREBP1c-CRY1 axis suppresses hepatic gluconeogenesis upon insulin. Cell Cycle *16*, 139–140.
13. Zhang, E.E., Liu, Y., Dentin, R., Pongsawakul, P.Y., Liu, A.C., Hirota, T., Nusinow, D.A., Sun, X., Landais, S., Kodama, Y., et al. (2010). Cryptochrome mediates circadian regulation of cAMP signaling and hepatic gluconeogenesis. Nat. Med. *16*, 1152–1156.
14. Lamia, K.A., Papp, S.J., Yu, R.T., Barish, G.D., Uhlenhaut, N.H., Jonker, J.W., Downes, M., and Evans, R.M. (2011). Cryptochromes mediate rhythmic repression of the glucocorticoid receptor. Nature *480*, 552–556.
15. Riddle, M.R., Aspiras, A.C., Gaudenz, K., Peuß, R., Sung, J.Y., Martineau, B., Peavey, M., Box, A.C., Tabin, J.A., McGaugh, S., et al. (2018). Insulin resistance in cavefish as an adaptation to a nutrient-limited environment. Nature *555*, 647–651.
16. Aspiras, A.C., Rohner, N., Martineau, B., Borowsky, R.L., and Tabin, C.J. (2015). Melanocortin 4 receptor mutations contribute to the adaptation of cavefish to nutrient-poor conditions. Proc. Natl. Acad. Sci. USA *112*, 9668–9673.
17. Mack, K.L., Jaggard, J.B., Persons, J.L., Roback, E.Y., Passow, C.N., Stanhope, B.A., Ferrufino, E., Tsuchiya, D., Smith, S.E., Slaughter, B.D., et al. (2021). Repeated evolution of circadian clock dysregulation in cavefish populations. PLoS Genet. *17*, e1009642.
18. Ceinos, R.M., Frigato, E., Pagano, C., Fröhlich, N., Negrini, P., Cavallari, N., Vallone, D., Fuselli, S., Bertolucci, C., and Foulkes, N.S. (2018). Mutations in blind cavefish target the light-regulated circadian clock gene, period 2. Sci. Rep. *8*, 8754.
19. Cavallari, N., Frigato, E., Vallone, D., Fröhlich, N., Lopez-Olmeda, J.F., Foà, A., Berti, R., Sánchez-Vázquez, F.J., Bertolucci, C., and Foulkes, N.S. (2011). A blind circadian clock in cavefish reveals that opsins mediate peripheral clock photoreception. PLoS Biol. *9*, e1001142.
20. Di Rosa, V., Frigato, E., Negrini, P., Cristiano, W., López-Olmeda, J.F., Rétaux, S., Sánchez-Vázquez, F.J., Foulkes, N.S., and Bertolucci, C. (2024). Sporadic feeding regulates robust food entrainable circadian clocks in blind cavefish. iScience *27*, 110171.
21. Ghosh, S., Lewis, K.N., Tulsian, R., Astafev, A.A., Buffenstein, R., and Kondratov, R.V. (2021). It's about time; divergent circadian clocks in the livers of mice and naked mole-rats. FASEB J. *35*, e21590.
22. Riccio, A.P., and Goldman, B.D. (2000). Circadian rhythms of locomotor activity in naked mole-rats (Heterocephalus glaber). Physiol. Behav. *71*, 1–13.
23. Avivi, A., Albrecht, U., Oster, H., Joel, A., Beiles, A., and Nevo, E. (2001). Biological clock in total darkness: the Clock/MOP3 circadian system of the blind subterranean mole rat. Proc. Natl. Acad. Sci. USA *98*, 13751–13756.
24. Avivi, A., Oster, H., Joel, A., Beiles, A., Albrecht, U., and Nevo, E. (2002). Circadian genes in a blind subterranean mammal II: Conservation and uniqueness of the three Period homologs in the blind subterranean mole rat, Spalax ehrenbergi superspecies. Proc. Natl. Acad. Sci. USA *99*, 11718–11723.
25. Avivi, A., Oster, H., Joel, A., Beiles, A., Albrecht, U., and Nevo, E. (2004). Circadian genes in a blind subterranean mammal III: molecular cloning and circadian regulation of cryptochrome genes in the blind subterranean mole rat, Spalax ehrenbergi superspecies. J. Biol. Rhythms *19*, 22–34.
26. Olsen, L., Krishnan, J., Banks, C., Hassan, H., and Rohner, N. (2023). Circadian rhythm disruption linked to skeletal muscle dysfunction in the Mexican Cavefish. Curr. Biol. *33*, R255–R256.
27. Xiong, S., Wang, W., Kenzior, A., Olsen, L., Krishnan, J., Persons, J., Medley, K., Peuß, R., Wang, Y., Chen, S., et al. (2022). Enhanced lipogenesis through Pparγ helps cavefish adapt to food scarcity. Curr. Biol. *32*, 2272–2280.e6.
28. Moran, D., Softley, R., and Warrant, E.J. (2014). Eyeless Mexican cavefish save energy by eliminating the circadian rhythm in metabolism. PLoS One *9*, e107877.
29. Bastiaanssen, T.F.S., Leigh, S.-J., Tofani, G.S.S., Gheorghe, C.E., Clarke, G., and Cryan, J.F. (2023). Kronos: A computational tool to facilitate biological rhythmicity analysis. Preprint at bioRxiv. https://doi.org/10.1101/2023.04.21.537503.
30. Okano, S. (2018). Unique Aspects of Cryptochrome in Chronobiology and Metabolism, Pancreatic β-Cell Dysfunction, and Regeneration: Research into Cysteine414-Alanine Mutant CRY1. J. Diabetes Res. *2016*, 3459246.
31. Walton, J.C., Bumgarner, J.R., and Nelson, R.J. (2022). Sex differences in circadian rhythms. Cold Spring Harb. Perspect. Biol. *14*, a039107.

32. Lok, R., Qian, J., and Chellappa, S.L. (2024). Sex differences in sleep, circadian rhythms, and metabolism: Implications for precision medicine. Sleep Med. Rev. *75*, 101926.

33. Preitner, N., Damiola, F., Lopez-Molina, L., Zakany, J., Duboule, D., Albrecht, U., and Schibler, U. (2002). The orphan nuclear receptor REV-ERBalpha controls circadian transcription within the positive limb of the mammalian circadian oscillator. Cell *110*, 251–260.

34. Annayev, Y., Adar, S., Chiou, Y.Y., Lieb, J.D., Sancar, A., and Ye, R. (2014). Gene Model 129 (Gm129) Encodes a Novel Transcriptional Repressor That Modulates Circadian Gene Expression. J. Biol. Chem. *289*, 5013–5024.

35. Cao, X., Yang, Y., Selby, C.P., Liu, Z., and Sancar, A. (2021). Molecular mechanism of the repressive phase of the mammalian circadian clock. Proc. Natl. Acad. Sci. USA *118*, e2021174118.

36. Kawamoto, T., Noshiro, M., Sato, F., Maemura, K., Takeda, N., Nagai, R., Iwata, T., Fujimoto, K., Furukawa, M., Miyazaki, K., et al. (2004). A novel autofeedback loop of Dec1 transcription involved in circadian rhythm regulation. Biochem. Biophys. Res. Commun. *313*, 117–124.

37. Sato, F., Kawamoto, T., Fujimoto, K., Noshiro, M., Honda, K.K., Honma, S., Honma, K.i., and Kato, Y. (2004). Functional analysis of the basic helix-loop-helix transcription factor DEC1 in circadian regulation. Interaction with BMAL1. Eur. J. Biochem. *271*, 4409–4419.

38. Meroni, G., Reymond, A., Alcalay, M., Borsani, G., Tanigami, A., Tonlorenzi, R., Lo Nigro, C., Messali, S., Zollo, M., Ledbetter, D.H., et al. (1997). Rox, a novel bHLHZip protein expressed in quiescent cells that heterodimerizes with Max, binds a non-canonical E box and acts as a transcriptional repressor. EMBO J. *16*, 2892–2906.

39. Scoma, H.D., Humby, M., Yadav, G., Zhang, Q., Fogerty, J., and Besharse, J.C. (2011). The de-ubiquitinylating enzyme, USP2, is associated with the circadian clockwork and regulates its sensitivity to light. PLoS One *6*, e25382.

40. Srikanta, S.B., Brown, T.W., Malescot, A., Cloutier, M.È., Zhu, L., Coutanson, C., Malki, M., Storch, K.F., Rungta, R., Cayouette, M., et al. (2025). The deubiquitinase USP2 modulates photic entrainment of the circadian clock at the level of the suprachiasmatic nucleus. J. Neurochem. *169*, e70018.

41. Srikanta, S.B., Stojkovic, K., and Cermakian, N. (2021). Behavioral phenotyping of mice lacking the deubiquitinase USP2. PLoS One *16*, e0241403.

42. Yang, Y., Duguay, D., Fahrenkrug, J., Cermakian, N., and Wing, S.S. (2014). USP2 Regulates the Intracellular Localization of PER1 and Circadian Gene Expression. J. Biol. Rhythms *29*, 243–256.

43. Gekakis, N., Staknis, D., Nguyen, H.B., Davis, F.C., Wilsbacher, L.D., King, D.P., Takahashi, J.S., and Weitz, C.J. (1998). Role of the CLOCK protein in the mammalian circadian mechanism. Science *280*, 1564–1569.

44. Ripperger, J.A., and Schibler, U. (2006). Rhythmic CLOCK-BMAL1 binding to multiple E-box motifs drives circadian Dbp transcription and chromatin transitions. Nat. Genet. *38*, 369–374.

45. Mokhosoev, I.M., Astakhov, D.V., Terentiev, A.A., and Moldogazieva, N.T. (2024). Cytochrome P450 monooxygenase systems: Diversity and plasticity for adaptive stress response. Prog. Biophys. Mol. Biol. *193*, 19–34.

46. Kriebs, A., Jordan, S.D., Soto, E., Henriksson, E., Sandate, C.R., Vaughan, M.E., Chan, A.B., Duglan, D., Papp, S.J., Huber, A.L., et al. (2017). Circadian repressors CRY1 and CRY2 broadly interact with nuclear receptors and modulate transcriptional activity. Proc. Natl. Acad. Sci. USA *114*, 8776–8781.

47. Hotamisligil, G.S., and Bernlohr, D.A. (2015). Metabolic functions of FABPs–mechanisms and therapeutic implications. Nat. Rev. Endocrinol. *11*, 592–605.

48. Khavandgar, Z., and Murshed, M. (2015). Sphingolipid metabolism and its role in the skeletal tissues. Cell. Mol. Life Sci. *72*, 959–969.

49. Sugden, M.C. (2003). PDK4: A factor in fatness? Obes. Res. *11*, 167–169.

50. Zi, Z., and Rao, Y. (2024). Discoveries of GPR39 as an evolutionarily conserved receptor for bile acids and of its involvement in biliary acute pancreatitis. Sci. Adv. *10*, eadj0146.

51. Nathanson, N.M. (1987). Molecular properties of the muscarinic acetylcholine receptor. Annu. Rev. Neurosci. *10*, 195–236.

52. Greve, S., Kuhn, G.A., Saenz-de-Juano, M.D., Ghosh, A., von Meyenn, F., and Giller, K. (2022). The major urinary protein gene cluster knockout mouse as a novel model for translational metabolism research. Sci. Rep. *12*, 13161.

53. Kirby, G.M., Nichols, K.D., and Antenos, M. (2011). CYP2A5 induction and hepatocellular stress: an adaptive response to perturbations of heme homeostasis. Curr. Drug Metab. *12*, 186–197.

54. Bauman, D.R., Steckelbroeck, S., Williams, M.V., Peehl, D.M., and Penning, T.M. (2006). Identification of the major oxidative 3alpha-hydroxysteroid dehydrogenase in human prostate that converts 5alpha-androstane-3alpha,17beta-diol to 5alpha-dihydrotestosterone: a potential therapeutic target for androgen-dependent disease. Mol. Endocrinol. *20*, 444–458.

55. Hu, P., Zhang, M., and Napoli, J.L. (2007). Ontogeny of rdh9 (Crad3) expression: ablation causes changes in retinoid and steroid metabolizing enzymes, but RXR and androgen signaling seem normal. Biochim. Biophys. Acta *1770*, 694–705.

56. Burris-Hiday, S.D., and Scott, E.E. (2021). Steroidogenic cytochrome P450 17A1 structure and function. Mol. Cell. Endocrinol. *528*, 111261.

57. Reue, K. (2009). The lipin family: mutations and metabolism. Curr. Opin. Lipidol. *20*, 165–170.

58. Li, J.-D., Burton, K.J., Zhang, C., Hu, S.B., and Zhou, Q.Y. (2009). Vasopressin receptor V1a regulates circadian rhythms of locomotor activity and expression of clock-controlled genes in the suprachiasmatic nuclei. Am. J. Physiol. Regul. Integr. Comp. Physiol. *296*, R824–R830.

59. Shebl, N., and Salama, M. (2025). Exploring dopa decarboxylase as an ideal biomarker in Parkinson's disease with focus on regulatory mechanisms, cofactor influences, and metabolic implications. NPJ Biomed. Innov. *2*, 2.

60. Li, Q., Zhang, S., Wang, H., Wang, Z., Zhang, X., Wang, Y., and Yuan, J. (2023). Association of rotating night shift work, CLOCK, MTNR1A, MTNR1B genes polymorphisms and their interactions with type 2 diabetes among steelworkers: a case-control study. BMC Genom. *24*, 232.

61. Amin, M., and Gragnoli, C. (2023). Melatonin receptor 1A (MTNR1A) gene linkage and association to type 2 diabetes in Italian families. Eur. Rev. Med. Pharmacol. Sci. *27*, 4688–4692.

62. Wang, H., Gauthier, B.R., Hagenfeldt-Johansson, K.A., Iezzi, M., and Wollheim, C.B. (2002). Foxa2 (HNF3beta) controls multiple genes implicated in metabolism-secretion coupling of glucose-induced insulin release. J. Biol. Chem. *277*, 17564–17570.

63. Wolfrum, C., Shih, D.Q., Kuwajima, S., Norris, A.W., Kahn, C.R., and Stoffel, M. (2003). Role of Foxa-2 in adipocyte metabolism and differentiation. J. Clin. Investig. *112*, 345–356.

64. Yabe, D., Brown, M.S., and Goldstein, J.L. (2002). Insig-2, a second endoplasmic reticulum protein that binds SCAP and blocks export of sterol regulatory element-binding proteins. Proc. Natl. Acad. Sci. USA *99*, 12753–12758.

65. Frese, M.-A., Schulz, S., and Dierks, T. (2008). Arylsulfatase G, a novel lysosomal sulfatase. J. Biol. Chem. *283*, 11388–11395.

66. Froy, O. (2009). Cytochrome P450 and the biological clock in mammals. Curr. Drug Metab. *10*, 104–115.

67. Estrella, M.A., Du, J., Chen, L., Rath, S., Prangley, E., Chitrakar, A., Aoki, T., Schedl, P., Rabinowitz, J., and Korennykh, A. (2019). The metabolites NADP+ and NADPH are the targets of the circadian protein Nocturnin (Curled). Nat. Commun. *10*, 2367.

68. Rosen, E.D., Sarraf, P., Troy, A.E., Bradwin, G., Moore, K., Milstone, D.S., Spiegelman, B.M., and Mortensen, R.M. (1999). PPAR gamma is

required for the differentiation of adipose tissue in vivo and in vitro. Mol. Cell *4*, 611–617.

69. Yu, J.E., Han, S.Y., Wolfson, B., and Zhou, Q. (2018). The role of endothelial lipase in lipid metabolism, inflammation, and cancer. Histol. Histopathol. *33*, 1–10.
70. Kelson, T.L., Secor McVoy, J.R., and Rizzo, W.B. (1997). Human liver fatty aldehyde dehydrogenase: microsomal localization, purification, and biochemical characterization. Biochim. Biophys. Acta *1335*, 99–110.
71. Fourcade, S., Ruiz, M., Camps, C., Schlüter, A., Houten, S.M., Mooyer, P.A.W., Pàmpols, T., Dacremont, G., Wanders, R.J.A., Giròs, M., and Pujol, A. (2009). A key role for the peroxisomal ABCD2 transporter in fatty acid homeostasis. Am. J. Physiol. Endocrinol. Metab. *296*, E211–E221.
72. Yu, S., Meng, S., Xiang, M., and Ma, H. (2021). Phosphoenolpyruvate carboxykinase in cell metabolism: Roles and mechanisms beyond gluconeogenesis. Mol. Metab. *53*, 101257.
73. Okar, D.A., Manzano, A., Navarro-Sabatè, A., Riera, L., Bartrons, R., and Lange, A.J. (2001). PFK-2/FBPase-2: maker and breaker of the essential biofactor fructose-2,6-bisphosphate. Trends Biochem. Sci. *26*, 30–35.
74. Zhang, Y., Xu, D., Huang, H., Chen, S., Wang, L., Zhu, L., Jiang, X., Ruan, X., Luo, X., Cao, P., et al. (2014). Regulation of glucose homeostasis and lipid metabolism by PPP1R3G-mediated hepatic glycogenesis. Mol. Endocrinol. *28*, 116–126.
75. Hanson, R.W., and Garber, A.J. (1972). Phosphoenolpyruvate carboxykinase. I. Its ce:role in gluconeogenesis. Am. J. Clin. Nutr. *25*, 1010–1021.
76. Jiang, X.-C. (2020). Impact of phospholipid transfer protein in lipid metabolism and cardiovascular diseases. Adv. Exp. Med. Biol. *1276*, 1–13.
77. Dean, M., Rzhetsky, A., and Allikmets, R. (2001). The human ATP-binding cassette (ABC) transporter superfamily. Genome Res. *11*, 1156–1166.
78. Tsui, H.S., Pham, N.V.B., Amer, B.R., Bradley, M.C., Gosschalk, J.E., Gallagher-Jones, M., Ibarra, H., Clubb, R.T., Blaby-Haas, C.E., and Clarke, C.F. (2019). Human COQ10A and COQ10B are distinct lipid-binding START domain proteins required for coenzyme Q function. J. Lipid Res. *60*, 1293–1310.
79. Reinke, H., and Asher, G. (2019). Crosstalk between metabolism and circadian clocks. Nat. Rev. Mol. Cell Biol. *20*, 227–241.
80. Mendoza, J. (2025). Brain circadian clocks timing the 24h rhythms of behavior. npj Biol. Timing Sleep *2*, 13.
81. Hirano, A., Braas, D., Fu, Y.H., and Ptáček, L.J. (2017). FAD regulates CRYPTOCHROME protein stability and circadian clock in mice. Cell Rep. *19*, 255–266.
82. Busino, L., Bassermann, F., Maiolica, A., Lee, C., Nolan, P.M., Godinho, S.I.H., Draetta, G.F., and Pagano, M. (2007). SCFFbxl3 controls the oscillation of the circadian clock by directing the degradation of cryptochrome proteins. Science *316*, 900–904.
83. Lee, C., Etchegaray, J.P., Cagampang, F.R., Loudon, A.S., and Reppert, S.M. (2001). Posttranslational mechanisms regulate the mammalian circadian clock. Cell *107*, 855–867.
84. Guan, D., Xiong, Y., Trinh, T.M., Xiao, Y., Hu, W., Jiang, C., Dierickx, P., Jang, C., Rabinowitz, J.D., and Lazar, M.A. (2020). The hepatocyte clock and feeding control chronophysiology of multiple liver cell types. Science *369*, 1388–1394.
85. Korenčič, A., Bordyugov, G., Košir, R., Rozman, D., Goličnik, M., and Herzel, H. (2012). The interplay of cis-regulatory elements rules circadian rhythms in mouse liver. PLoS One *7*, e46835.
86. Joye, D.A.M., and Evans, J.A. (2022). Sex differences in daily timekeeping and circadian clock circuits. Semin. Cell Dev. Biol. *126*, 45–55.
87. Bur, I.M., Cohen-Solal, A.M., Carmignac, D., Abecassis, P.Y., Chauvet, N., Martin, A.O., van der Horst, G.T.J., Robinson, I.C.A.F., Maurel, P., Mollard, P., and Bonnefont, X. (2009). The circadian clock components CRY1 and CRY2 are necessary to sustain sex dimorphism in mouse liver metabolism. J. Biol. Chem. *284*, 9066–9073.
88. Aherrahrou, R., Kulle, A.E., Alenina, N., Werner, R., Vens-Cappell, S., Bader, M., Schunkert, H., Erdmann, J., and Aherrahrou, Z. (2020). CYP17A1 deficient XY mice display susceptibility to atherosclerosis, altered lipidomic profile and atypical sex development. Sci. Rep. *10*, 8792.
89. Gul, S., Aydin, C., Ozcan, O., Gurkan, B., Surme, S., Baris, I., and Kavakli, I.H. (2020). The Arg-293 of Cryptochrome1 is responsible for the allosteric regulation of CLOCK-CRY1 binding in circadian rhythm. J. Biol. Chem. *295*, 17187–17199.
90. Okano, S., Akashi, M., Hayasaka, K., and Nakajima, O. (2009). Unusual circadian locomotor activity and pathophysiology in mutant CRY1 transgenic mice. Neurosci. Lett. *451*, 246–251.
91. Patke, A., Murphy, P.J., Onat, O.E., Krieger, A.C., Özçelik, T., Campbell, S.S., and Young, M.W. (2017). Mutation of the human circadian clock gene CRY1 in familial delayed sleep phase disorder. Cell *169*, 203–215.e13.
92. Jang, H., Lee, G.Y., Selby, C.P., Lee, G., Jeon, Y.G., Lee, J.H., Cheng, K. K.Y., Titchenell, P., Birnbaum, M.J., Xu, A., et al. (2016). SREBP1c-CRY1 signalling represses hepatic glucose production by promoting FOXO1 degradation during refeeding. Nat. Commun. *7*, 12180.
93. Swaminathan, A., Xia, F., and Rohner, N. (2024). From darkness to discovery: evolutionary, adaptive, and translational genetic insights from cavefish. Trends Genet. *40*, 24–38.
94. Beale, A., Guibal, C., Tamai, T.K., Klotz, L., Cowen, S., Peyric, E., Reynoso, V.H., Yamamoto, Y., and Whitmore, D. (2013). Circadian rhythms in Mexican blind cavefish Astyanax mexicanus in the lab and in the field. Nat. Commun. *4*, 2769.
95. Frøland Steindal, I.A., Beale, A.D., Yamamoto, Y., and Whitmore, D. (2018). Development of the Astyanax mexicanus circadian clock and non-visual light responses. Dev. Biol. *441*, 345–354.
96. Xiong, S., Krishnan, J., Peuß, R., and Rohner, N. (2018). Early adipogenesis contributes to excess fat accumulation in cave populations of Astyanax mexicanus. Dev. Biol. *441*, 297–304.
97. Bano-Otalora, B., Moye, M.J., Brown, T., Lucas, R.J., Diekman, C.O., and Belle, M.D. (2021). Daily electrical activity in the master circadian clock of a diurnal mammal. eLife *10*, e68179.
98. Börding, T., Abdo, A.N., Maier, B., Gabriel, C., and Kramer, A. (2019). Generation of Human CRY1 and CRY2 Knockout Cells Using Duplex CRISPR/Cas9 Technology. Front. Physiol. *10*, 577.
99. Stemmer, M., Thumberger, T., Del Sol Keyer, M., Wittbrodt, J., and Mateo, J.L. (2015). CCTop: An Intuitive, Flexible and Reliable CRISPR/Cas9 Target Prediction Tool. PLoS One *10*, e0124633.
100. Connelly, J.P., and Pruett-Miller, S.M. (2019). CRIS.py: A Versatile and High-throughput Analysis Program for CRISPR-based Genome Editing. Sci. Rep. *9*, 4194.
101. Dobin, A., Davis, C.A., Schlesinger, F., Drenkow, J., Zaleski, C., Jha, S., Batut, P., Chaisson, M., and Gingeras, T.R. (2013). STAR: ultrafast universal RNA-seq aligner. Bioinformatics *29*, 15–21.
102. Li, B., and Dewey, C.N. (2011). RSEM: accurate transcript quantification from RNA-Seq data with or without a reference genome. BMC Bioinf. *12*, 323.
103. Labuhn, M., Adams, F.F., Ng, M., Knoess, S., Schambach, A., Charpentier, E.M., Schwarzer, A., Mateo, J.L., Klusmann, J.H., and Heckl, D. (2018). Refined sgRNA efficacy prediction improves large- and small-scale CRISPR–Cas9 applications. Nucleic Acids Res. *46*, 1375–1385.

STAR★METHODS

KEY RESOURCES TABLE

REAGENT or RESOURCE	SOURCE	IDENTIFIER
Antibodies		
Guinea pig polyclonal anti-CRY1 (diluted 1:1000)	MBL International	Cat#PM081
Mouse monoclonal anti-GAPDH (diluted 1:10000)	Proteintech	Cat#60004-1-Ig; RRID:AB_2107436
Rabbit polyclonal anti-H3 polyclonal antibody (diluted 1:10000)	Abcam	Cat#ab1791; RRID:AB_302613
Donkey anti-Guinea Pig IgG secondary antibody (diluted 1:4000)	LiCOR	Cat#926-68007
Donkey anti-Mouse IgG secondary antibody (1:10000)	LiCOR	Cat#926-32212
Donkey anti-Rabbit IgG secondary antibody (1:10000)	LiCOR	Cat#926-68073
Chemicals, peptides, and recombinant proteins		
Alt-R S.p. HiFi Cas9 nuclease V3	Integrated DNA Technologies	Cat#1081059
Pregnant mare serum gonadotropin (PMSG)	Genway Biotech	Cat#GWB-2AE30A
Chorionic gonadotropin human (hCG)	Millipore	Cat#C1063-1VL
EmbryoMax KSOM Mouse Embryo Media	Millipore	Cat#MR-106-D
(DMEM), high glucose, GlutaMAX^{TM} supplement	Gibco	Cat#10566016
Radioimmunoprecipitation Assay (RIPA) Buffer	ThermoFisher Scientific	Cat#89900
0.45 μm PVDF membrane	Merck	Cat#IVPH00010
Precision Plus Protein Dual Color Standards	Bio-Rad	Cat#1610374
20% glucose solution	Gibco	Cat#A24940-01
TRIzol reagent	ThermoFisher Scientific	Cat#15596026
DNase I	New England Biolabs	Cat#M0303S
Critical commercial assays		
ProNex Size-Selective Purification System	Promega	Cat#NG2002
DNeasy Blood and Tissue Kit	Qiagen	Cat#69504
Pierce BCA Assay	ThermoFisher Scientific	Cat#23227
Monarch Spin RNA Cleanup Kit (500 μg)	New England Biolabs	Cat#T2050L
NEBNext Ultra II Directional RNA Library Prep Kit for Illumina	New England Biolabs	Cat#E7760L
NEBNext Poly(A) mRNA Magnetic Isolation Module	New England Biolabs	Cat#E7490L
NEBNext Multiplex Oligos for Illumina	New England Biolabs	Cat#E6440S
NEBNext Poly(A) mRNA Magnetic Isolation Module	New England Biolabs	Cat# E7490L
SPRISelect	Beckman Coulter	Cat#B23318
SG Library Compatibility Kit	Singular Genomics	Cat#700141
Cell Line Nucleofector Kit V	Lonza Bioscience	Cat#VCA-1003
Deposited data		
Metabolic phenotyping (indirect calorimetry) dataset	This paper	Stowers Original Data Repository https://www.stowers.org/research/publications/libpb-2490
RNA-seq dataset	This paper	Raw FASTQ files: Gene Expression Omnibus (GEO): GSE277611; analysis code: Stowers Original Data Repository https://www.stowers.org/research/publications/libpb-2490

(*Continued on next page*)

Continued

REAGENT or RESOURCE	SOURCE	IDENTIFIER
List of genomic locations occupied by CRY1 and nuclear receptors	Kriebs et al.[46]	N/A
Experimental models: Cell lines		
U-2 OS BLH CRY1/2 double KO cell line	Dr. Achim Kramer, described in Börding et al.[98]	N/A
Experimental models: Organisms/strains		
CRY1 R263Q strain	This paper	N/A
Oligonucleotides		
Alt-R HDR Donor Oligo (Sequence 5′GCCCAACTG GACTCAGTCCTTATCTCCGCTTTGGTTGTCTGTCC TGTCAGCTGTTTTATTTCAAACTAACAGAT CTCTACAAAAAGgtattatctgaag3′)	Integrated DNA Technologies	N/A
Alt-R CRISPR-Cas9 sgRNA (Sequence 5′GCTTTGGTTGTTTATCATGT3′)	Integrated DNA Technologies	N/A
CRY1 R263Q genotyping forward primer (Sequence 5′AGGCCTGGGTGGC AAACTTTG3′)	Integrated DNA Technologies	N/A
CRY1 R263Q genotyping reverse primer (Sequence 5′CGCCACAGGAGTT GCCCATAAA3′)	Integrated DNA Technologies	N/A
Recombinant DNA		
pMC1SG5 vector	Dr. Aziz Sancar, plasmid described in Ye et al.[4]	N/A
Software and algorithms		
CCTop	Stemmer et al.[99]	N/A
CRIS.py	Connelly et al.[100]	N/A
Macro Interpreter V24.1.0	Sable Systems	N/A
One Click Macro V2.53.2-slice15min and V2.53.2-slice1hr	Sable Systems	N/A
sgdemux 1.2.0	Bioconda	https://github.com/Singular-Genomics/singular-demux
Kronos package	Bastiaanssen et al.[29]	https://github.com/thomazbastiaanssen/kronos
bcl-convert version 3.10.5	Illumina	https://emea.support.illumina.com/sequencing/sequencing_software/bcl-convert.html
STAR aligner version 2.7.10b	Dobin et al.[101]	https://github.com/alexdobin/STAR
RSEM version 1.3.1	Li and Dewey[102]	https://github.com/deweylab/RSEM
edgeR version 3.42.4	Bioconductor	https://bioconductor.org/packages/release/bioc/html/edgeR.html
clusterProfiler version 4.8.2	Bioconductor	https://bioconductor.org/packages/release/bioc/html/clusterProfiler.html
AnnotationHub version 3.8.0	Bioconductor	https://bioconductor.org/packages/release/bioc/html/AnnotationHub.html

EXPERIMENTAL MODEL AND STUDY PARTICIPANT DETAILS

Mouse strains

All experiments were performed in strict accordance with the guidelines of the Institute Animal Care and Use Committees (IACUCs) of the Stowers Institute and the University of Kansas Medical Center (KUMC). CRISPR-Cas9 technology was used for engineering C57BL6/J mice. Potential guide RNA target sites were designed using CCTop.[99] The target site was selected by evaluating the predicted on-target efficiency score and the off-target potential[103] in addition to the proximity of the double-stranded break to the desired mutation site. To generate the R263Q codon change, a single-stranded DNA oligonucleotide (ssODN) donor was designed

containing ~50 nucleotides of homology from the double-stranded break site. The ssODN contained mutations for the R263Q change as well as silent codon changes to disrupt guide RNA binding following the repair event. The ssODN was ordered as an Alt-R HDR Donor Oligo from Integrated DNA Technologies (IDT). The selected guide RNA was ordered as an Alt-R CRISPR-Cas9 sgRNA from IDT. Figure S1A provides a graphic summary of the CRISPR design.

3–4-week-old C57BL6/J females were super-ovulated using pregnant mare serum gonadotropin (PMSG) given at noon, followed by human chorionic gonadotropin (HCG) 46 h later at 10:00 a.m., and then paired with C57BL6/J stud males overnight. All females with copulation plugs the next morning were kept and used to harvest embryos. Harvested embryos were placed in potassium-supplemented simplex optimized medium (KSOM) and incubated until electroporation was performed.

A ribonucleoprotein (RNP) complex was formed by incubating sgRNA at 6 μM final concentration with IDT Cas9 HiFi v3 protein at 1.2 μM final concentration at room temperature for 10 min. The ssODN was added at 200 ng/μL final concentration to the RNP. Eighty-four fertilized embryos were selected and electroporated with the RNP complex using the Nepa Gene electroporator. After electroporation, embryos were transferred into recipient females. These females carried the embryos to term and gave birth to pups which were screened for the expected mutations by lysing an ear clip and amplifying the specific genomic location. A second round of amplification was performed to incorporate sample-specific dual barcodes. All amplicons were pooled and size-selected using ProNex Size-Selective Purification System (NG2002, Promega). Cleaned pools were quantified on a Qubit Fluorimeter and then run on a Bioanalyzer (Agilent) to check sizing and purity. Purified pools were run on an Illumina MiSeq 2x250 flow cell. The resulting sequence data were demultiplexed, and read pairs were joined. On-target indel frequency and expected mutations were analyzed using CRIS.py.[100]

Founder males were chosen to be paired with C57BL6/J wild-type females to create the F1 generation. The pups resulting from these matings were weaned and sequenced as described above for the founders. Any positive pups with confirmed germline transmission were kept as F1s. When these mice reached breeding age (6–8 weeks) they were set up with new C57BL6/J wild-type mice to produce the F2 generation that contained heterozygotes. Heterozygotes were crossed with each other to produce the F3 generation with litters containing wild-type mice and mice homozygous for the introduced mutation. Since large numbers of animals were required for achieving adequately powered statistical analyses for our metabolic experiments, and due to the high usage and the limited availability of reservations on the indirect calorimeter, CRY1 WT mice were derived by crossing wild-type mice and the CRY1 R263Q mice were derived by crossing mutant mice. For experiments performed at the Stowers Institute for Medical Research, mice were housed in a 14:10 light/dark cycle (lights on at 5:45 a.m. and off at 7:45 p.m.) with food (Teklad 2020X, Inotiv) and water available *ad libitum*. For experiments performed at KUMC, mice were housed in a 12:12 light/dark cycle (lights on at 6:00 a.m. and off at 6:00 p.m.) with food (Teklad 8604, Inotiv) and water available *ad libitum* during quarantine periods and experiments. All experiments used adult mice from both genotypes (WT and CRY1 R263Q homozygote) aged between 2 and 4 months. To account for possible sex differences, each experiment used both male and female mice from both genotypes. Analyses of sex-based differences can be found in the results and discussion sections.

Cell lines

U-2 OS BLH CRY1/2 KO cell lines were cultured in Dulbecco's Modified Eagle Medium (DMEM), high glucose, GlutaMAX supplement (10566016, Gibco) supplemented with 10% fetal bovine serum (FBS), 25 mM HEPES, 1X PenStrep and 1X Trypsin-EDTA at 37°C and 5% CO_2. Confluent cells were transiently transfected with the pMC1SG5 vector (see the key resources table) using the Cell Line Nucleofector Kit V (VCA-1003, Lonza Bioscience) according to the manufacturer's instructions. The cell line has been tested for mycoplasma contamination, and authenticated by STR profiling (ATCC HTB-96) and as described in Börding et al.[98]

METHOD DETAILS

PCR genotyping

DNA was extracted from ear biopsies using the Qiagen DNeasy Blood and Tissue Kit (69504, Qiagen) following the manufacturer's instructions. The site of the CRY1 R263Q mutation was amplified for 35 cycles using a forward primer sequence 5′AGGCCTGGGTGGCAAACTTTG3′ and a reverse primer sequence 5′CGCCACAGGAGTTGCCCATAAAG3'. The primers were designed to amplify a 300 bp fragment flanking the mutation site and spanning the entire ssODN sequence to ensure that the amplification is from the *Cry1* locus and not from elsewhere in the genome. The denaturation, annealing and extension steps were carried out for 30, 30 and 60 s respectively, at 95°C, 60°C and 72°C respectively. PCR amplicons were Sanger sequenced to identify WT and R263Q mutant samples. Figure S1B shows example Sanger sequencing chromatograms comparing the site of mutation in a WT individual with a CRY1 R263Q homozygote.

Tissue lysis and western blotting

3 mice per experimental group (WT female, R263Q female, WT male and R263Q male) aged between 3 and 4 months were euthanized with CO_2 followed by cervical dislocation. Livers were harvested from each mouse, washed in 1X PBS, and fragments of the largest lobe of each liver were flash frozen in liquid nitrogen. Tissue harvesting was done between ZT12 and ZT13 (onset of the dark phase). For total protein extracts, liver fragments were thawed on ice and then homogenized in 20 μL of radioimmunoprecipitation assay (RIPA) buffer (89900, ThermoFisher Scientific) per mg of tissue, using a Type A Dounce homogenizer on ice. Protein

concentrations were determined using the BCA assay (23227, Pierce) following the manufacturer's instructions. Samples were incubated at 70°C for 10 min with 4X Laemmli buffer and then loaded on a 10% polyacrylamide/SDS gel for electrophoresis. The separated proteins were transferred to a 0.45 μm PVDF membrane (IVPH00010, Merck) at a constant voltage of 25 V for 2 h. Post-transfer, the membrane was washed thrice with TBS-Tw (1X TBS with 0.1% v/v Tween 20) and blocked for 1 h with a blocking buffer (5% w/v instant nonfat dry milk in TBS-Tw). Primary antibodies were diluted in blocking buffer and incubated with the membrane for 2 h. Following primary antibody incubation, the membrane was washed thrice with TBS-Tw and then incubated with secondary antibodies diluted in the blocking buffer for 1 h, then washed thrice. Imaging was carried out on the LiCOR Odyssey CLx system. All steps in the western blotting protocol after transfer were carried out at room temperature. The primary and secondary antibodies and the dilutions used can be found in the key resources table.

Indirect calorimetry data acquisition

Mice aged 3–4 months were transferred from the Stowers Institute to the KUMC Metabolic Core and placed under quarantine for 14 days. Upon release from quarantine, mice were housed individually for 7 days to reduce stress prior to calorimetry. Mice were then placed into standard cages in an indirect calorimetry system (Promethion, Sable Systems, Las Vegas, NV) to measure whole body energy expenditure/metabolism, and voluntary movement/activity (see Figure 2A for a graphic summary of the procedure). Mice were acclimated for 3–4 days in the system prior to study data collection. After the acclimation period, data were collected and analyzed with Macro Interpreter (V24.1.0) in 15-min and 1-h increments using a One Click Macro provided by Sable Systems (V.2.53.2-slice15min and V.2.53.2-slice1hr, respectively). Measurements were obtained from 44 individuals aged 3–4 months spread over three experimental cohorts. Cohort 1 consisted of 16 individuals (4 WT females, 4 R263Q females, 4 WT males and 4 R263Q males) measured for 17 full days, Cohort 2 comprised 12 individuals (same as Cohort 1 but no R263Q females included) measured for 8 full days, and Cohort 3 consisted of 16 individuals (6 WT females, 6 R263Q females and 4 R263Q males) measured for 9 full days. Each shipment of mice and each run on the indirect calorimeter was designed to include WT and R263Q groups from each sex whenever available to ensure that control and mutant animals were subjected to the same quarantine and experimental regimen and to minimize batch effects.

Glucose tolerance testing

Mice aged 2 months were fasted for about 6 h to acquire fasting blood glucose measurements. Before the start of the experiment, each mouse was weighed and then tail veins were pricked to draw blood that was used to measure fasting blood glucose levels using an Alpha Trak 3 glucometer and test strips. Mice were then injected intraperitoneally with 2 mg/g of body weight of glucose (A24940-01, Gibco) administered as 10 μL per g of body weight of a 20% w/v glucose solution. Postprandial blood glucose levels were then measured at 10, 20, 30, 60 and 120 min post glucose injection. Experiments were done using 33 mice in 3 independent cohorts, and then pooled for plotting and analysis, with individuals from each experimental group represented in each cohort. A graphic summary of the glucose tolerance testing procedure is provided in Figure S5C.

RNA extraction and sequencing

Mice aged between 3 and 4 months were euthanized with CO_2 followed by cervical dislocation. Brains and livers were harvested and washed in 1X PBS. The left hemisphere of each brain, and fragments of the largest lobe of each liver were immediately homogenized in TRIzol reagent (15596026, ThermoFisher Scientific) using a tissue homogenizer (Z742682, Sigma) with 1.5 mm zirconium beads. Tissue harvesting was done at two ZTs – between ZT12 and ZT13 (onset of the dark phase) and between ZT22 and ZT23 (onset of the light phase). For samples collected at the onset of the light phase, n = 6 WT female brain samples, 5 R263Q female brain samples, 5 WT male brain samples, 6 R263Q male brain samples, 5 WT female liver samples, 6 R263Q female liver samples, 5 WT male liver samples, and 5 R263Q male liver samples. For samples collected at the onset of the dark phase, n = 4 WT female brain samples, 4 R263Q female brain samples, 6 WT male brain samples, 5 R263Q male brain samples, 5 WT female liver samples, 5 R263Q female liver samples, 7 WT male liver samples, and 6 R263Q male liver samples. RNA was extracted following the manufacturer's instructions. The extracted RNA samples were treated with DNase I (M0303S, New England Biolabs) and then purified using the NEB Monarch Spin RNA Cleanup Kit (T2050, New England Biolabs) following the manufacturer's instructions.

mRNAseq libraries were generated from 500 ng of high-quality total RNA, as assessed using the Bioanalyzer (Agilent), according to the manufacturer's directions using a 5-fold dilution of the universal adaptor and 9 cycles of PCR per the respective masses with the NEBNext Ultra II Directional RNA Library Prep Kit for Illumina (NEB, E7760L), the NEBNext Poly(A) mRNA Magnetic Isolation Module (NEB, E7490L), and the NEBNext Multiplex Oligos for Illumina (96 Unique Dual Index Primer Pairs) (NEB, E6440S) and purified using the SPRIselect bead-based reagent (Beckman Coulter, B23318). The resulting short fragment libraries were checked for quality and quantity using the Bioanalyzer (Agilent) and Qubit Flex Fluorometer (Life Technologies). Equal molar libraries were pooled, quantified, and converted to process on the Singular Genomics G4 with the SG Library Compatibility Kit, following the "Adapting Libraries for the G4 – Retaining Original Indices" protocol. The converted pools were sequenced on F2 flow cells (700101) on the G4 instrument with the PP1 and PP2 custom index primers included in the SG Library Compatibility Kit (700141), using Instrument Control Software 23.08.1–1 with the following read lengths: 8 bp Index1, 50 bp Read1, 8 bp Index2, and 50 bp Read2. Following sequencing, sgdemux 1.2.0 was run to demultiplex reads for all libraries and generate FASTQ files.

QUANTIFICATION AND STATISTICAL ANALYSIS

Indirect calorimetry data analysis

All data processing, analysis and plotting steps were carried out in RStudio (version 4.4.0). 15-min increment measurements for energy expenditure (EE) in kcal/h, locomotor activity in beam breaks per interval and respiratory exchange ratio (RER) obtained from Sable Systems Macro Interpreter were used to derive hourly measurements for each cohort of mice. The measurements for feeding counts were recorded by the calorimeter as individual occurrences for each individual. These occurrences were converted to hourly frequencies. The hourly data for each cohort were trimmed on both ends to include only those experiment days for which all measurements were available from 12:00 a.m. to 11:59 p.m. The hourly data were then averaged by ZT across all days to generate tables for each cohort providing hourly measurements for each ZT (0–23) that had been averaged over several experimental days. The tables for the 3 cohorts were pooled into a single larger table. For each individual, hourly values were summed over the light period (ZT0-11), dark period (ZT12-23), or over the entire 24-h day to get average values of each parameter over a photoperiod (light period, dark period or 24-h day).

To compare 24-h EE profiles, the first analysis was done using the R package Kronos[29] that is designed for circadian time series analyses, to assess the circadian rhythmicity of the data and compare rhythmicity between groups. The second analysis was performed by fitting an ANOVA model with covariates to compare 24-h EE profiles. The details of covariate choice are explained in the results section.

RNA-seq data analysis

Samples from each ZT were collected, sequenced and analyzed separately. Raw reads were demultiplexed into FASTQ files using Illumina's bcl-convert (version 3.10.5) before being aligned to UCSC genome GRCm39 with STAR aligner (version 2.7.10b), using Ens_110 gene models. TPM values were generated using RSEM (version 1.3.1). The STAR read counts table was used for differential gene expression analysis using edgeR package (version 3.42.4) in RStudio (R version 4.3.1). Lowly expressed genes were filtered out with filterByExpr's default settings followed by a trimmed mean of M-values (TMM) normalization. The edgeR design matrix was designed to account for batch effects between sequencing runs. Differential gene expression comparisons were performed between genotypes (WTand R263Q) but within the same sex, tissue type and ZT. Genes showing absolute values of log2 fold change > 0.585 (or absolute values of fold change >1.5) and adjusted p-values less than 0.05 were identified as differentially expressed. Up- and down-regulated gene lists from each comparison were used as input for Gene Ontology (GO term) pathway enrichment analysis. GO term enrichment was completed using TERMS2GO, an in-house R Shiny app (versions R 4.3.1, shiny 1.7.5). Significant gene ontology terms were identified using clusterProfiler's enrichGO function (version 4.8.2) with AnnotationHub's species database (version 3.8.0). GO Terms with adjusted p-values less than 0.05 were considered significant (Fisher's exact test). Figures were generated using ggplot2 (version 3.4.3) and plotly (4.10.2).

Statistical analyses

All statistical analyses were carried out in RStudio (version 4.4.0). For indirect calorimetry analyses, analysis of variance (ANOVA) was used to determine covariates contributing to differences between WT and R263Q mutant 24-h profile datasets. Following this, an ANOVA model with covariates was fitted to the data to obtain p-values comparing WT and R263Q individuals at every ZT. Raw p-values were adjusted using the Bonferroni correction for 24 hypotheses. Adjusted p-values less than 0.05 were considered significant. For glucose tolerance testing, for comparing the timing of the second peaks in EE/activity in the dark phase and for comparing EE/activity/feeding/RER values over a photoperiod, the non-parametric Wilcoxon test was used to obtain p-values which were considered significant when less than 0.05. For all statistical analyses, the statistical parameters are provided in the results section and in the figure legends.